NeuroImage 328 (2026) 121758

Contents lists available at ScienceDirect

NeuroImage

journal homepage: www.elsevier.com/locate/ynimg

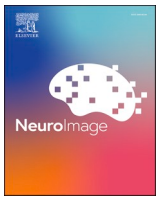

Human frontopolar cortex plays a causal role in decomposing high-dimensional information during decision making

Chun-Kit Law [a,*], Nicole H.L. Wong [a], Jing Jun Wong [a], Evelyn Y.H. Huang [a], Rongjun Yu [b], Bolton K.H. Chau [a,c,d]

[a] Department of Rehabilitation Sciences, The Hong Kong Polytechnic University, Hong Kong
[b] Department of Education and Psychology, Academy of Wellness and Human Development, Faculty of Arts and Social Sciences, Hong Kong Baptist University, Hong Kong
[c] University Research Facility in Behavioral and Systems Neuroscience, The Hong Kong Polytechnic University, Hong Kong
[d] Mental Health Research Centre, The Hong Kong Polytechnic University, Hong Kong

ARTICLE INFO

Keywords:
Frontopolar cortex
Area 10
Anterior prefrontal cortex
Decision making
High-dimensional choice information

ABSTRACT

Humans navigate in complex environments with abundant information. However, it is unclear how the human brain involves specific mechanisms to extract meaningful features from high-dimensional information to guide adaptive decision making. Here, we focused on investigating the causal role of the lateral frontopolar cortex (FPl), an area uniquely evolved in the human brain, in decomposing high-dimensional choice information. This was achieved via three experiments that collectively involved transcranial magnetic stimulation (TMS), resting-state functional magnetic resonance imaging (fMRI), task-based fMRI, and computational modelling. First, we found that disrupting FPl using TMS with a continuous theta-burst stimulation (cTBS) protocol impaired decision making with high-dimensional, but not low-dimensional, information. Second, we developed a computational model that arbitrates between a multi-feature decomposition mechanism and a simple heuristic. This model aided explaining that the FPl-TMS effect was attributed to diminished capabilities in multi-feature decomposition. Finally, fMRI data revealed stronger intrinsic FPl signals were related to greater tendency of employing multi-feature decomposition. Together, our results suggest a causal role of FPl in extracting decision-related features from high-dimensional information.

1. Introduction

Human is particularly good at making sense of complex, high-dimensional information, which is important to making adaptive decisions in the human-shaped environment. For example, investing in stock requires decomposing months or years of daily stock price into useful features for guiding decisions, such as the average price, risk, and occurrence of extreme events. There has been great interest in studying neuroeconomic processes shared amongst primate species. However, how the human prefrontal cortex has developed specific mechanisms for solving human-shaped neuroeconomic problems is broadly unclear. To address this theoretical gap, one reasonable approach is to focus on investigating brain regions that are well-developed in the human brain, relative to other primate brains. The lateral subdivision of the frontopolar cortex (FPl) is a good candidate because it is considered a uniquely developed region of the human brain due to its sulcal morphology and connectivity fingerprint (Amiez et al., 2023; Neubert et al., 2015, 2014). Recently, there is also a growing interest in stimulating the frontopolar cortex for treating psychiatric disorders (Soleimani et al., 2024). Hence, the current study focuses on studying the specific role of the human FPl in decision making.

Intriguingly, FPl activity was reported in decision-making processes shared amongst other primate species, which raises questions about the unique function of the human FPl. For example, it was found that the FPl signals exploration and counterfactual information while humans were performing a decision-making task (Boorman et al., 2011, 2009; Daw et al., 2006; Raja Beharelle et al., 2015). However, similar signals can also be found in the human dACC (Boorman et al., 2011; Doll et al., 2015; Kolling et al., 2012) or the macaque dACC (Blanchard and Hayden, 2014; Fouragnan et al., 2019; Hayden et al., 2011) when both species were given a similar task. Although it is unclear what are the specific neuroeconomic functions of the human FPl, it appears it is

* Corresponding author.
E-mail address: kelvinck.law@gmail.com (C.-K. Law).

https://doi.org/10.1016/j.neuroimage.2026.121758
Received in revised form 13 January 2026; Accepted 26 January 2026
Available online 1 February 2026

related to handling of information in changing environments.

Given that the human environment is abundant in information, we hypothesize that the FPl is involved in decomposing high-dimensional information for guiding economic choices. This hypothesis is supported by a few views. In brief, one view suggests that the FPl enables cognitive branching - the ability to put one task on hold and resume it later, while being interrupted by a second task (Koechlin, 2014, 2011). Another theory suggests that the FPl is involved in using analogy or analogical reasoning - the ability to identify similarities between abstract features and to generalize that to new cases (Aichelburg et al., 2016; Urbanski et al., 2016; Volle et al., 2010). A third view suggest that the FPl is involved in abstract rule switching (Badre and Nee, 2018; Nee and D'Esposito, 2016). Arguably, one commonality of these three views is that the process involved in the FPl should involve combining information into meaningful features to inform decision making.

Here, we probed the causal role and the precise mechanistic processes of the FPl, a unique region of the human brain, in decomposing high-dimensional information during decision making. Three key questions to address are: (1) Does disruption of FPl lead to impaired decision making with high-dimensional information? (2) How is high-dimensional information decomposed for guiding decision making? (3) Can FPl's functional profile be explained by the decomposition of high-dimensional information? To investigate the underlying mechanism, we performed three experiments that collectively involved a combination of transcranial magnetic stimulation (TMS), resting-state functional magnetic resonance imaging (fMRI), task-based fMRI, and computational modelling. Our analyses yielded four key findings. First, disrupting the FPl using TMS impaired decision making only when participants encountered high-dimensional, but not low-dimensional, information (Experiment 1). Second, we established a computational model that describes individuals' extent of using a multi-feature extraction process versus a heuristic of simple averaging for digesting choice information (Experiment 2) and this model was robust across all three experiments that involved FPl-TMS, fMRI, or without any TMS or fMRI. Third, by applying the computational model, we showed mechanistically that the disruption in high-dimensional choice after FPl-TMS was due to a shift from the multi-feature extraction to simple heuristic (Experiments 1 and 2). Finally, individuals who showed stronger signals in the FPl also used the multi-feature extraction to a larger extent (Experiments 2 and 3). These convergent findings provide causal evidence showing the mechanism of the FPl for digesting high-dimensional information during decision making.

2. Results

2.1. Impaired high-dimensional choice after FPl disruption

How FPl mechanistically decomposes and integrates the high-

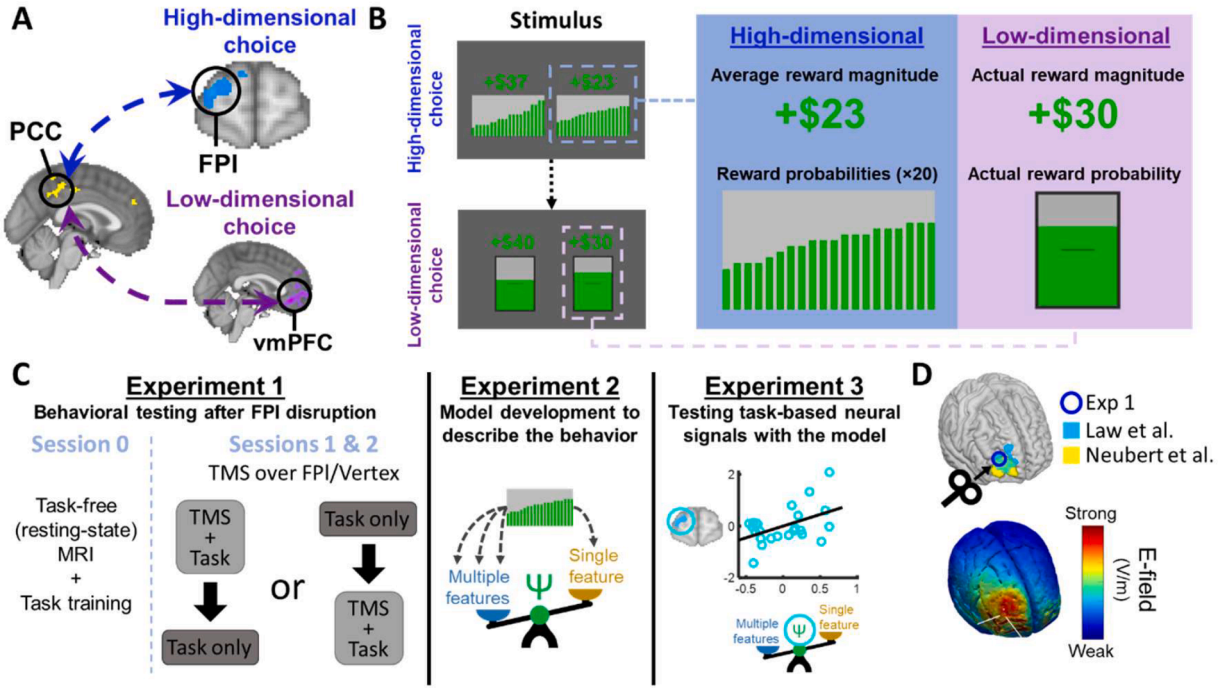

Fig. 1. Study design. (A) Previous findings revealed a double dissociation of FPl and vmPFC in high-dimensional choice and low-dimensional choice respectively, and PCC flexibly communicated with FPl/vmPFC to guide high-/low-dimensional choice (Law et al., 2023). (B) A two-stage decision making task. Each block began with a Stage 1 high-dimensional choice trial, followed by Stage 2 low-dimensional choice trials. On each Stage 1 trial, participants chose between two high-dimensional options. Each high-dimensional option was composed of twenty low-dimensional gambles. The reward probabilities of these twenty gambles were represented by the heights of twenty bars and their average reward magnitude was represented by a number. After choosing a high-dimensional option, two component gambles from which were pseudo-randomly drawn. Participants had to choose between these two low-dimensional gambles and then a probabilistic reward was delivered subsequently. (C) This study involved three experiments. In Experiment 1, participants received resting-state functional MRI scanning, experienced a taster session of the TMS pulses, and performed a practice run to familiarize with the experimental task in Session 0. Sessions 1 and 2 were the TMS sessions in which participants performed the task after TMS or performed the task without TMS. TMS was applied over the key FPl region or the control vertex region. The order of TMS conditions (TMS or no TMS) and TMS region was counterbalanced across participants. In Experiment 2, different computational models were developed for describing the mechanistic processes underlying high-dimensional choice and how they were impaired after TMS. In Experiment 3, the best-fitting computational model developed in Experiment 2 was further used to explain FPl's activities during high-dimensional choice. (D) (Top panel) The stimulation position of FPl in Experiment 1 was defined based on the coordinates that are implicated in decision making with high-dimensional information (Law et al., 2023). It also overlaps with the area of FPl that is suggested to be unique in hominid species (Neubert et al., 2015). (Bottom panel) The simulated electric field (E-field) centred at the stimulation position of FPl. White bars represent the distances of the stimulation position away from the scalp ($X = 80.4121 \pm 1.9954$; $Y = 127.1519 \pm 1.6541$; $Z = 21.2643 \pm 2.4483$).

dimensional information into meaningful features for decision making remains highly unclear despite the neuroimaging findings showing that FPl passes digested high-dimensional choice information to posterior cingulate cortex (PCC) for guiding decision making (Law et al., 2023) (Fig. 1. A). In this study, we further examined the causal role of FPl in digesting high-dimensional choice information and its precise computational mechanisms. To this end, we first tested whether and how disruption of FPl would impair high-dimensional choice behavior. In Experiment 1, participants were required to perform a two-stage decision making task, in which choices in Stage 1 involved high-dimensional information and choices in Stage 2 involved low-dimensional information. Specifically, Stage 1 involved choosing between two collections of gambles (Fig. 1. B, S1). Each collection involved high-dimensional information of twenty gambles - individual probabilities of the twenty gambles and the average reward magnitude of these gambles. After choosing a collection, from which two gambles were randomly drawn and offered subsequently in Stage 2. Each of these low-dimensional gambles in Stage 2, similar to many typical studies (e.g., Hunt et al., 2012; Jocham et al., 2014; Kolling et al., 2014; Strait et al., 2014), was associated with certain levels of reward probability and magnitude. High-dimensional choice in Stage 1 therefore required digesting and integrating multifaceted information. A simulation was run and the results confirm that the best strategy in Stage 1 to maximize reward involves considering the variance and skewness of the reward probabilities (Fig. S2). To examine the causal role of the FPl in high-dimensional choice, participants received TMS, using a continuous theta-burst stimulation (cTBS) protocol, to disrupt their FPls before performing the task (Fig. 1. C, D). On another day, they underwent an active control condition where they received TMS over the vertex. On both days, participants also performed the task with no prior TMS as additional control conditions. The sequence of the conditions (TMS vs no TMS; FPl vs vertex) was counterbalanced across participants.

A general linear model (GLM) was first performed to test participants' use of choice information to guide their decisions. We regressed participants' high-dimensional choices against the reward magnitude and the mean, variance, and skewness of the reward probabilities. As expected, participants preferred options with greater reward magnitudes (i.e., $Rew_{(R-L)}$; $\beta s > 2.5397$, $ps < 3.6554 \times 10^{-8}$; Fig. 2. A, left panel) and greater mean reward probabilities (i.e., $Prob\text{-}Mean_{(R-L)}$; $\beta s > 1.4511$, $ps < 3.7845 \times 10^{-9}$; Fig. 2. A, left panel). They also preferred greater variances of the reward probabilities (i.e., $Prob\text{-}Variance_{(R-L)}$; $\beta s > 0.1631$, $ps < 0.0386$; Fig. 2. A, left panel) in all conditions, although no effect of the skewness of the reward probabilities was observed (i.e., $Prob\text{-}Skewness_{(R-L)}$; $\beta s < 0.1009$, $ps > 0.2172$; Fig. 2. A, left panel). The Stage 2 low-dimensional choices were tested by regressing against the differences in reward magnitude and reward probability between the options. Not surprisingly, participants preferred options with greater reward magnitudes (i.e., $Rew_{(R-L)}$; $\beta s > 2.7045$, $ps < 1.7908 \times 10^{-10}$; Fig. 2. A, right panel) and reward probabilities (i.e., $Prob_{(R-L)}$; $\beta s > 3.8345$, $ps < 2.3205 \times 10^{-9}$; Fig. 2. A, right panel).

We next turned to examine whether participants made less optimal choices on high-dimensional choice trials but not low-dimensional choice trials, after the FPl was disrupted. This was tested via a repeated measures three-way ANOVA [Region (FPl vs Vertex),

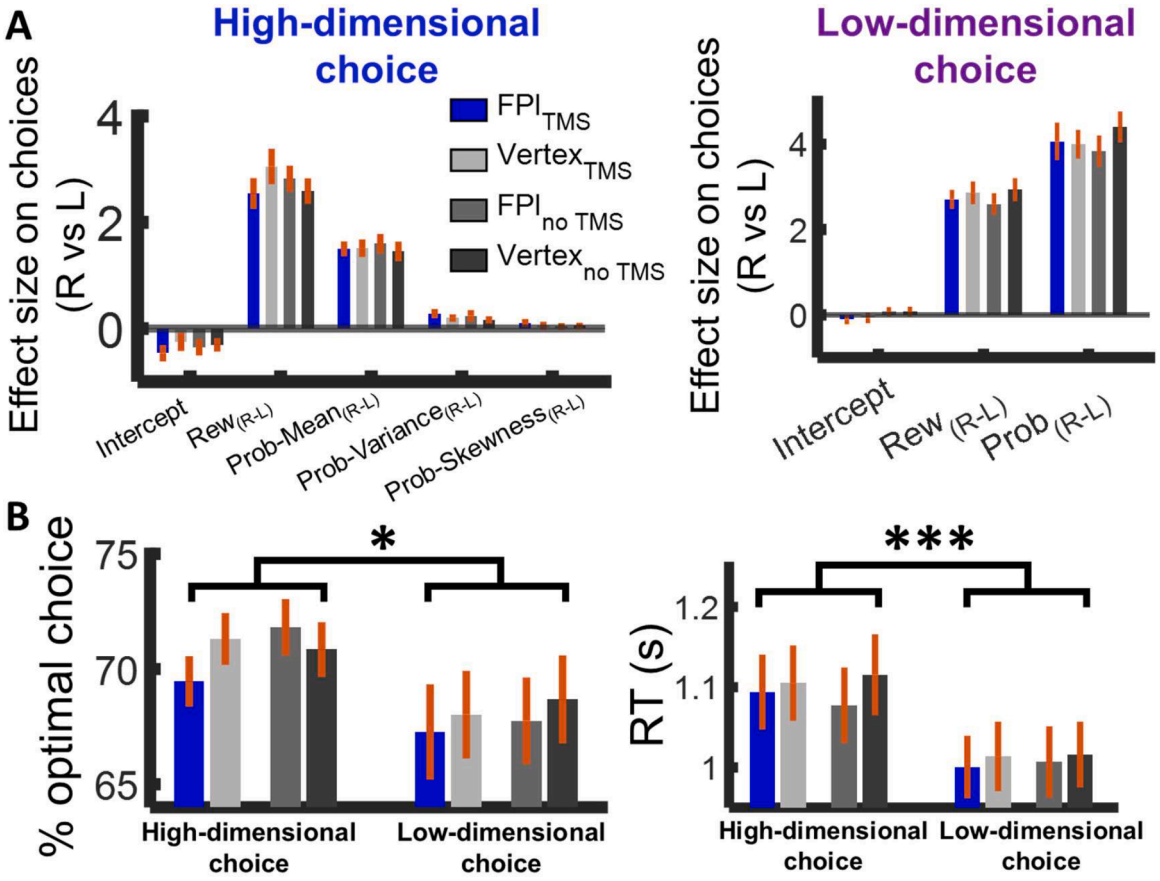

Fig. 2. Impairment in high-dimensional choice after FPl-TMS. (A) A logistic regression revealed that participants' choices were guided by the options' reward magnitude and reward probability, in both high-dimensional and low-dimensional choices. (B) (Left panel) However, on the high-dimensional choice trials, the percentage optimal choice was significantly lower on TMS trials than no-TMS trials in the FPl session. In contrast, the percentage optimal choice was comparable between the TMS and no TMS trials in the control Vertex session. On low-dimensional choice trials, there was a lack of TMS effect on both FPl and Vertex sessions. (Right panel) Participants also made slower responses in high-dimensional choice than low-dimensional choice. Error bars represent mean ± SEM. *$p < 0.05$ for the Region × Stimulation × Choice type interaction.

Stimulation (TMS vs no-TMS), and Choice type (high-dimensional vs low-dimensional)] on participants' percentage optimal choice data, in which optimal choice was defined according to the normative expected value (EV). We observed a significant Region × Stimulation × Choice type interaction (F (1,17) = 5.1316, p = 0.0368, η^2_P = 0.2319; Fig. 2. B, left panel, Table S1). A post hoc analysis showed that in the FPl session participants made less optimal choice on TMS trials than no-TMS trials during high-dimensional choice (F (1) = 4.4687, p = 0.0496, FWER-corrected p = 0.0883; Table S1). In contrast, in the vertex session participants' proportions of optimal choice were comparable on TMS and no-TMS trials (F (1) = 0.1756, p = 0.6807, FWER-corrected p = 0.8849; Table S1). The same post hoc analyses were applied to the low-dimensional choice and not surprisingly there was no significant difference between the TMS trials and no-TMS trials in the FPl session (F (1) = 2.8023, p = 0.1124, FWER-corrected p = 0.3639; Table S1) or in the vertex session (F (1) = 0.5730, p = 0.4595, FWER-corrected p = 0.8369; Table S1). Crucially, this specific FPl-TMS effect on impairing high-dimensional choice, but not low-dimensional choice, could not be explained away by any difference in difficulty level between high-dimensional choice and low-dimensional choice, because the overall percentages of optimal choice were comparable in the two stages (F (1,17) = 1.2614, p = 0.2770, η^2_P = 0.0691). Notably, two controlling factors were included as covariates in the ANOVA as the variances in these factors could potentially confound the results. Figure S3 shows the correlations between the choice accuracy and the covariates. First, reaction time, which could account for influences on choice accuracy due to the speed-accuracy trade-off. Indeed, we found that participants responded more slowly in high-dimensional choice than low-dimensional choice (t_{26} = 6.2241, p = 1.3847 × 10^{-6}; Fig. 2. B, right panel). Second, the peak resting-state functional connectivity (rsFC) between FPl and PCC. The FPl-PCC functional coupling was found selectively facilitating high-dimensional, but not low-dimensional, choice (Law et al., 2023). Moreover, TMS efficacy was found to be correlated with the intrinsic functional connectivity of the target region with its functionally coupled regions (Fox et al., 2012; Hawco et al., 2018), which makes it highly variable across individuals. We repeated the ANOVA without the covariates and showed that the specific FPl-TMS effect on impairing high-dimensional choice would be obscured by the covariates as the Region × Stimulation × Choice type interaction became non-significant after covariates removal (Table S1). To further confirm the reliability of this interaction during high-dimensional choice, we conducted a post-hoc power analysis. The results showed that the sample size was sufficient to detect the effect (η^2_P = 0.2319, α = 0.05, power = 1.0000).

In light of the role of PCC in utilizing the digested information from FPl to guide decision making and its functional-coupling with FPl during high-dimensional choice (Law et al., 2023), and greater efficacy of TMS is related to stronger intrinsic functional connectivity (Fox et al., 2012;

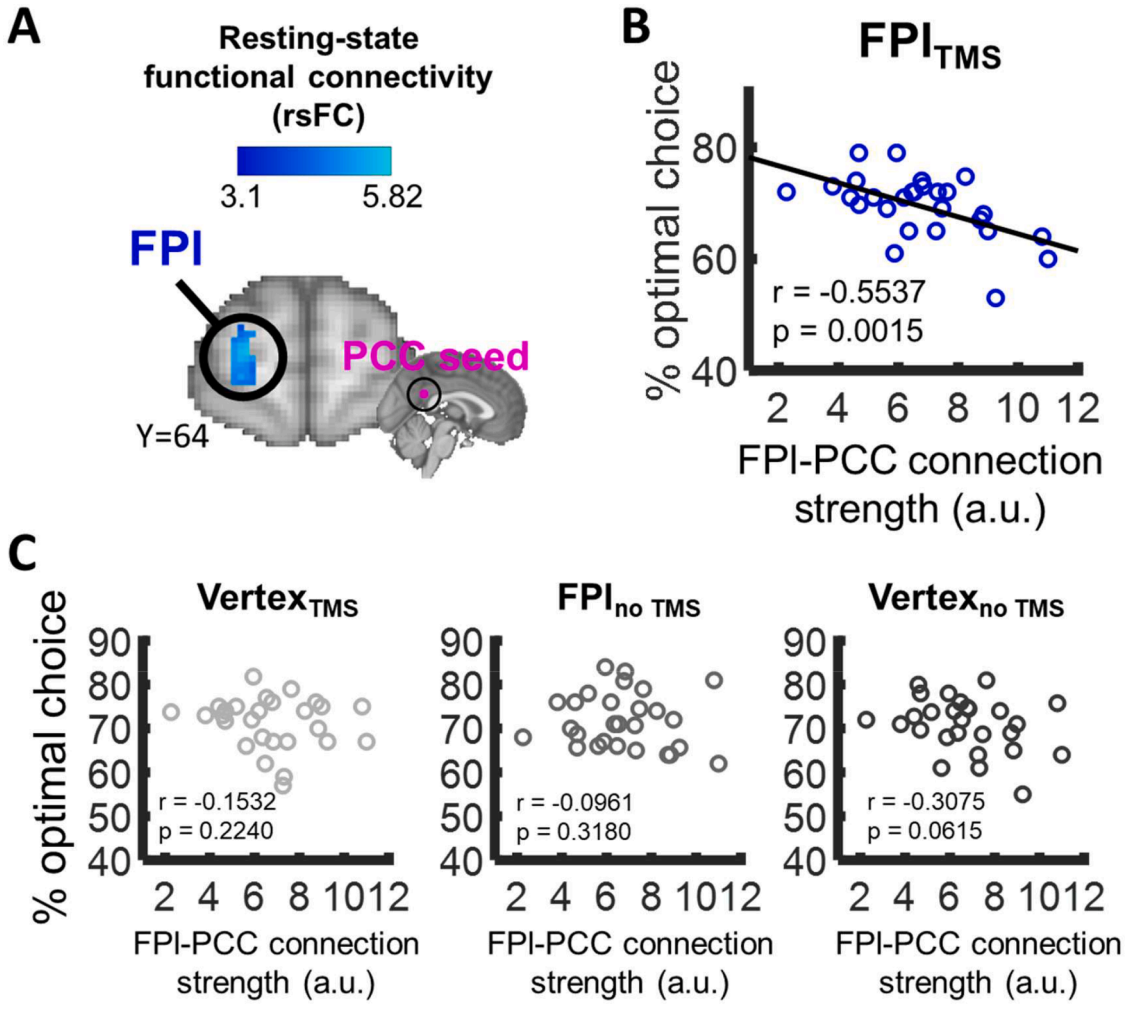

Fig. 3. Crucial role of FPl-PCC connection in high-dimensional choice. (A) A whole-brain resting-state functional connectivity analysis revealed FPl and PCC were intrinsically connected. For illustration purpose, a FPl mask (Neubert et al., 2015) was applied to indicate the area-of-interest in (B) and (C). (B) Crucially, after FPl-TMS, participants with stronger intrinsic FPl-PCC connectivity showed larger impairment in high-dimensional choice. (C) Such relationship was absent in all control conditions.

Hawco et al., 2018), we estimated the degree in which FPl and PCC were functionally connected using each participant's rsFC data (cluster-based thresholding $Z > 3.1$, $p < 0.0001$; Fig. 3. A) and tested whether that was also related to the extent of TMS effect. We found that participants with greater FPl-PCC connectivity exhibited fewer optimal choices after FPl-TMS ($r = -0.5537$, permutation $p = 0.0015$; Fig. 3. B), while such relationship was absent in all three control conditions ($|r|s < 0.3075$, permutation $ps > 0.0614$; Fig. 3. C). In contrast, in low-dimensional choice a correlation between FPl-PCC connectivity and optimal choice was absent in all four conditions (Fig. S4). These results support the notion that high-dimensional choice involves not only the FPl *per se*, but also its connection with the PCC.

2.2. Developing computational models for understanding the FPl-TMS effect mechanistically

Thus far we showed that disruption of FPl resulted in impaired high-dimensional choice by demonstrating less optimal choices. However, the precise computational mechanism of FPl in high-dimensional choice remains unclear. To tackle this problem, we need computational models for describing the mechanistic processes of making high-dimensional choice. To this end, we conducted Experiment 2, an experiment using the same behavioral task without any TMS or fMRI, and went through a two-phase model development.

In the Phase I model development, we considered that the space of model development should involve two sets of functions - attribute functions and integration functions (see Experiment 2 - *Modelling integration process of high-dimensional information* in Methods for details). In brief, the attribute functions account for possible ways by which choice attributes (i.e., reward magnitude and reward probability) are represented. They include (1) a linear function that keeps the magnitude and probabilities untransformed and then averages the probabilities; (2) a non-linear (nl) function that transforms the attributes and then averages the probabilities; (3) a multi-feature (MF) function that involves parallel decompositions of high-dimensional attribute components into multiple low-dimensional distribution parameters (i.e., the mean, variance, and skewness); (4) a nl-MF function involves non-linear transformation of the attributes prior the application of the MF.

Next, we also considered three possible ways in which reward magnitude and probabilities could be integrated. First, via a multiplicative function by calculating the product of reward magnitude and probability. Second, via an additive function that combines the reward magnitude and probability via a weighted-sum procedure. Third, a combination of both multiplicative and additive procedures.

Altogether, the four attribute functions and three integration functions produce twelve models (Fig. 4). Note that the normative EV model for defining optimal choice in Fig. 2. B is the same as the model that consists of a linear attribution function and a multiplicative integration function.

We fitted participants' high-dimensional choice data of Experiment 2 with all the twelve models and compared their goodness-of-fit using Bayesian model selection. The results revealed the $\text{Composite}_{\text{nl-MF}}$

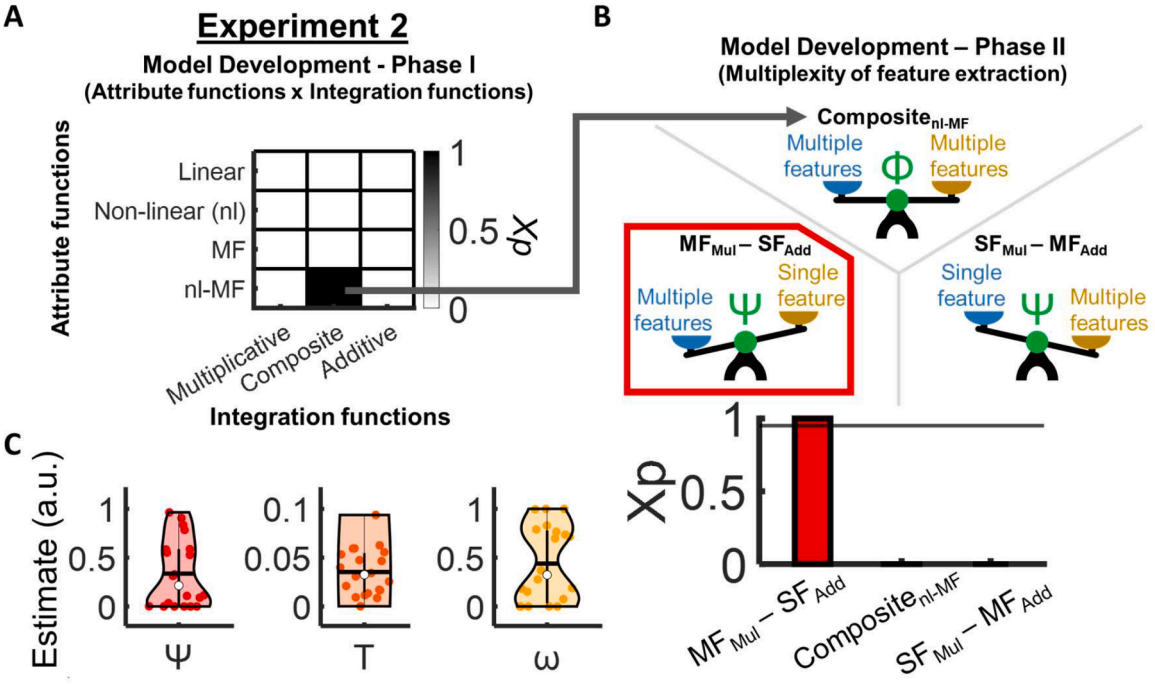

Fig. 4. High-dimensional choice is best described by a model that arbitrates between a multi-feature extraction process and a simple heuristic. (A) In the first phase of model development, we applied twelve models (by combining four attribute functions × three integration functions) to the data of Experiment 2, in which participants performed high-dimensional choices without receiving TMS. Specifically, each model consists of attribution functions to model how the choice attributes are represented. Each model also consists of an integration function to model how the choice attributes are integrated (either by addition, multiplication or a composite of both). Particularly, the composite integration function involves an integration coefficient (Φ) for controlling the arbitration between the multiplicative and additive integration. A Bayesian model selection showed that the $\text{Composite}_{\text{nl-MF}}$ model (with attribute functions of nl and MF, and a composite integration function) outperforms the other alternative models. MF = multi-feature extraction; nl-MF = *a* combined use of nl and MF. *Xp* = exceedance probability. (B) In the second phase of model development, the $\text{Composite}_{\text{nl-MF}}$ model (middle) was further adapted into two alternative models. The MF_{Mul} - SF_{Add} model keeps the multi-feature extraction process in the multiplicative arm whereas the additive arm involves a simple heuristic that only extracts single feature (left). In contrast, the SF_{Mul} - MF_{Add} model involves a simple heuristic in the multiplicative arm while keeping the multi-feature extraction in the additive arm (right). In these two variants, the arbitration between the multi-feature and single-feature arms is controlled by a multiplex coefficient (Ψ). A Bayesian model selection showed that the MF_{Mul} - SF_{Add} model outperforms the previously winning $\text{Composite}_{\text{nl-MF}}$ model in describing high-dimensional choice behavior in Experiment 2 (bottom panel). (C) Violin plots showing the fitted parameters of the winning MF_{Mul} - SF_{Add} model of individual participants. Vertical black lines represent the interquartile range. Horizontal black lines represent the mean. White circles represent the median. T = softmax temperature; ω = magnitude/probability weighting.

model significantly outperforms all other models (estimated frequency $Ef = 0.9563$; exceedance probability $Xp = 1.0000$; Fig. 4. A), suggesting that the high-dimensional choice attributes were non-linearly transformed and decomposed into multiple features of summary statistics (e.g., the mean, variance, skewness). Intriguingly, the results also revealed participants arbitrated between two integration strategies in parallel, which are the multiplicative approach and additive approach. Together, we showed that the $Composite_{nl-MF}$ model provides the best account of participants' high-dimensional choice behavior - a model that involves considering choice attributes non-linearly, decomposing high-dimensional information into multiple digested parameters (i.e., mean, variance and skewness), and arbitrating between additive and multiplicative integration strategies.

Phase I model development provided the foundation for representing and integrating choice attributes. To further examine the refined computations underlying the decomposition of high-dimensional information, we performed the Phase II model development. The winning $Composite_{nl-MF}$ model involves a push-pull mechanism of arbitrating between a multiplicative approach and an additive approach for information integration. The balance between the two strategies is controlled by an integration coefficient. However, in light of the presumed role of FPl in processing high-dimensional choice information, we hypothesized that to better account for FPl's function, the push-pull system should instead arbitrate between a multi-feature extraction process and a simple heuristic. To this end, we further developed two variants of the $Composite_{nl-MF}$ model. One variant, the MF_{Mul} - SF_{Add} model, involves keeping the multi-feature extraction (i.e., decomposing the high-dimensional reward probabilities into the mean, variance, and skewness) in the multiplicative arm and simplifying the additive arm by a simple heuristic (i.e., decomposing the reward probabilities into the mean only) (Fig. 4. B, left). As such, the additive arm no longer decomposes the high-dimensional information into multiple features, but just into a single feature of the mean. Another variant, the SF_{Mul} - MF_{Add} model, involves keeping the multi-feature extraction in the additive arm and simplifying the multiplicative arm by the single mean feature (Fig. 4. B, right). Importantly, in both models, the balance between the multi-feature extraction and simple heuristic processes is controlled by a multiplex coefficient Ψ.

We fitted the two variant models to the Experiment 2 data and compared their goodness-of-fit with the previously winning $Composite_{nl-MF}$ model. The MF_{Mul} - SF_{Add} model was found outperforming the other models in describing the high-dimensional choice behavior (estimated frequency $Ef = 0.8657$; exceedance probability $Xp = 1.0000$; Fig. 4. B, bottom panel). We also performed a model recovery analysis and a parameter recovery analysis to show that the MF_{Mul} - SF_{Add} model is stable (Fig. S5). Fig. 4C shows each participants' fitted parameters of the MF_{Mul} - SF_{Add} model, including the multiplex coefficient Ψ, softmax temperature T, and magnitude/probability weighting ω. The winning of the MF_{Mul} - SF_{Add} model suggests that participants' high-dimensional choice behavior was better described by the arbitration between a multi-feature extraction process and a simple heuristic process.

2.3. FPl disruption inhibits the multi-feature extraction process

So far, we have demonstrated that high-dimensional choice was disrupted by FPl-TMS (Fig. 2). However, it remains unclear what precise mechanistic processes were disrupted by FPl-TMS. With the findings of Experiment 2 that high-dimensional choice without TMS is best described by a push-pull mechanism that arbitrates between the multi-feature extraction and simple heuristic processes (Fig. 4), two explanatory hypotheses can be tested. First, FPl disruption resulted in a completely different strategy of information integration, i.e., behavior after FPl-TMS was best described by a different model. Alternatively, the same strategy remained after FPl-TMS, but the computational parameters of that strategy were altered.

To test which hypothesis was the case, we repeated the same model comparison procedures as in Fig. 4, but now using data from the four conditions of Experiment 1. For the first twelve models, we found that the $Composite_{nl-MF}$ model best describes high-dimensional choice behavior in all four TMS conditions (estimated frequency $Efs > 0.9672$; exceedance probability $Xps = 1.0000$; Fig. 5. A). Next, we further compared the goodness of fit of the $Composite_{nl-MF}$ model with the variants: the MF_{Mul} - SF_{Add} and SF_{Mul} - MF_{Add} models. We found that the MF_{Mul} - SF_{Add} model best describes high-dimensional choice behavior in all TMS conditions (estimated frequency $Efs > 0.8526$; exceedance probability $Xps = 1.0000$; Fig. 5. B). The winning MF_{Mul} - SF_{Add} model also outperforms all alternative models in terms of log likelihood (LL), area under the curve (AUC), prediction accuracy, and a hierarchical Bayesian's exceedance probability (Fig. S6). Our findings precluded the first hypothesis that FPl disruption resulted in a switch in strategy (i.e., a change in the best fit model), but instead participants continued to use the same strategy after FPl-TMS. We therefore examined more closely the computational parameters of the best-fit MF_{Mul} - SF_{Add} model across the four TMS conditions to test the second hypothesis - whether FPl disruption altered computational parameters.

Figs. 6A-C show participants' computational parameters of the MF_{Mul} - SF_{Add} model in the four TMS conditions in Experiment 1 (also see Table S2). To test the hypothesis that FPl disruption altered the computational parameters, each parameter was analyzed using a repeated measures three-way ANOVA [Region (FPl vs vertex), Stimulation (TMS vs no-TMS), and Choice type (high-dimensional vs low-dimensional)], controlled for model prediction accuracy (because it is interrelated to the estimates of the computational parameters) and reaction time (because there was significant difference between high-dimensional and low-dimensional choices; Fig. 2. B, right panel) to account for individual differences.

The ANOVA was first applied to test the multiplex coefficient. We found that there was a significant Region × Stimulation × Choice type interaction ($F(1,10) = 12.9461$, $p = 0.0049$, $\eta^2_P = 0.5642$; Table S1). A closer inspection on the high-dimensional choices alone revealed there was a significant Region × Stimulation interaction on the multiplex coefficient ($F(1,18) = 10.8105$,$p = 0.0041$, $\eta^2_P = 0.3752$; Fig. 6. A). In contrast, this Region × Stimulation interaction was absent in the low-dimensional choices ($F(1,18) = 3.5250$, $p = 0.0768$, $\eta^2_G = 0.1638$; Fig. S7, left panel). A post hoc analysis further showed that the multiplex coefficient was significantly smaller (i.e., participants became more likely to use a simple heuristic) after TMS was applied to FPl than the control vertex during high-dimensional choice ($F(1) = 16.8819$, $p = 0.0007$, FWER-corrected $p = 0.0039$; Table S1), whereas there was no significant difference in multiplex coefficient in the no-TMS condition during the FPl and vertex sessions during high-dimensional choice ($F(1) = 1.8450$, $p = 0.1911$, FWER-corrected $p = 0.6004$; Table S1). We also repeated the ANOVA without controlling for the confounding factors of model prediction accuracy and reaction time and showed that the specific FPl-TMS effect on the reduction in multiplex coefficient was obscured (Fig. S3, Table S1). To further confirm the reliability of the Region × Stimulation × Choice type interaction on multiplex coefficient during high-dimensional choice, we conducted a post-hoc power analysis. The results showed that the sample size was sufficient to detect the effect ($\eta^2_P = 0.5642$, $\alpha = 0.05$, power = 1.0000). The results remained similar when we focused on the Region × Stimulation interaction during high-dimensional choice alone ($\eta^2_P = 0.3752$, $\alpha = 0.05$, power = 1.0000). We found no significant Region × Stimulation × Choice type interaction effect on the softmax temperature parameter (although approaching significance; $F(1,10) = 4.0795$, $p = 0.0710$, $\eta^2_P = 0.2897$) and magnitude/probability weighting parameter ($F(1,10) = 1.3511$, $p = 0.2721$, $\eta^2_G = 0.1190$). Taken together, these results support our second hypothesis that FPl-TMS disrupted specific computational parameter by shifting the multiplex coefficient, instead of qualitatively switching participants' choice strategy.

In addition, we applied the fitted parameters of each participant back to the best-fit models and generated simulated choice data for each TMS

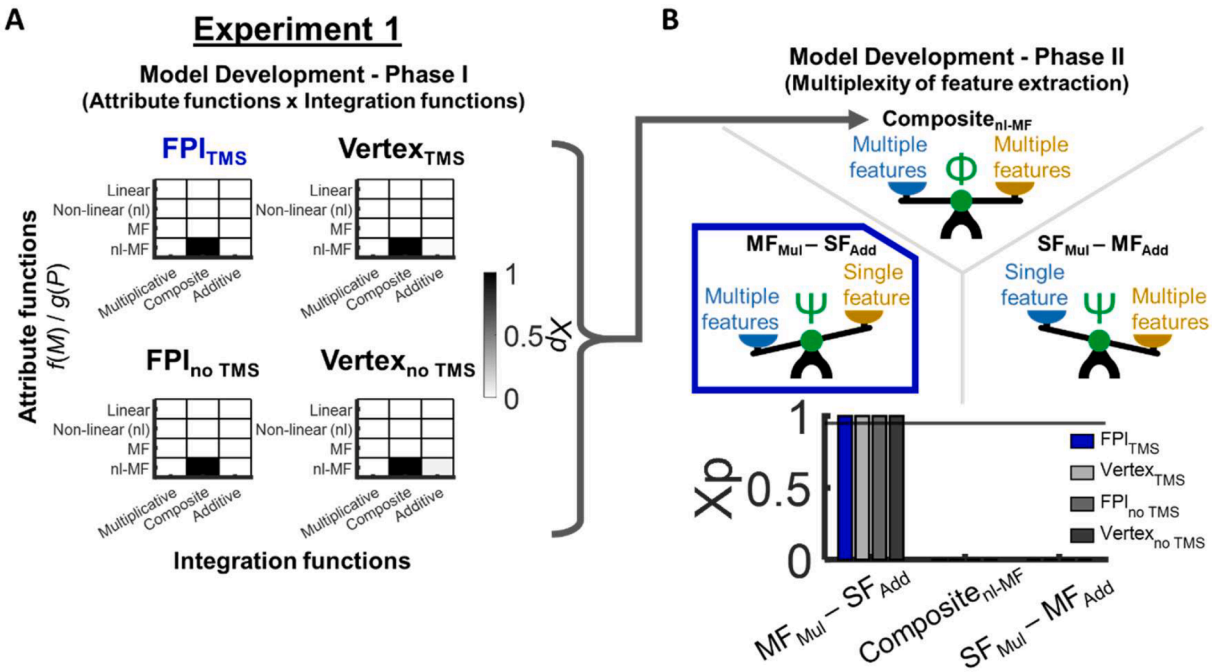

Fig. 5. The MF_{Mul} - SF_{Add} model best describes high-dimensional choice behavior in Experiment 1 that consisted of four TMS conditions. The same model development procedures as those for the Experiment 2 data were applied to the Experiment 1 data. (A) Participants' high-dimensional choice behavior in all conditions was best described by the $Composite_{nl-MF}$ model in the first phase of model development. This was the case even for the FPl-TMS condition that showed an impairment in high-dimensional choice. (B) In the second phase of model development that focuses on the multiplexity of the feature extraction process, the MF_{Mul} - SF_{Add} model outperforms the previously winning $Composite_{nl-MF}$ model in all conditions. MF = multi-feature extraction; nl-MF = *a* combined use of nl and MF. *Xp* = exceedance probability.

condition. In other words, we applied the MF_{Mul} - SF_{Add} model to generate high-dimensional choice and $Composite_{nl}$ model to generate low-dimensional choice. We estimated the percentage of optimal choice and analyzed that using the same three-way ANOVA. Consistent with Fig. 2B that involved empirical choice data, these simulated data showed a significant Region × Stimulation × Choice type interaction (F (1,17) = 5.1600, p = 0.0364, η^2_P = 0.2329). This suggested that the fitted parameters were able to capture the TMS effect on impairing optimal choice in the presence of high-dimensional information.

Subsequent between-participant analyses provide further support that the impaired optimal choice due to FPl-TMS (Fig. 2. B) was related to the disruption of a multi-feature extraction process. Here, we calculated the deviation in percentage of optimal choice, as well as the deviation in computational parameters, after FPl-TMS from the control condition of no-TMS in the FPl session. Crucially, we found that participants with greater reductions in multiplex coefficient after FPl-TMS also exhibited greater impairments in percentage optimal choice (r = 0.4089, permutation p = 0.0181) and no such significant deviation was found in the vertex session (r = 0.1340, permutation p = 0.2652). Interestingly, the deviation in percentage optimal choice showed a significant correlation with the deviation in softmax temperature (FPl_{TMS} - $FPl_{no\ TMS}$: r = −0.3693, permutation p = 0.0336; $Vertex_{TMS}$ - $Vertex_{no\ TMS}$: r = −0.0614, permutation p = 0.3464), suggesting those who became more stochastic after FPl-TMS also showed more impaired optimal choices. Finally, the impairment in percentage optimal choice was unrelated to the deviation in magnitude/probability weighting (FPl_{TMS} - $FPl_{no\ TMS}$: r = −0.0617, permutation p = 0.3949; $Vertex_{TMS}$ - $Vertex_{no\ TMS}$: r = −0.1036, permutation p = 0.3073). These results remained similar when each correlation between the choice data and a model parameter was orthogonalized with respect to the other two model parameters (multiplex coefficient [FPl_{TMS} - $FPl_{no\ TMS}$]: r = 0.4494, permutation p = 0.0110; multiplex coefficient [$Vertex_{TMS}$ - $Vertex_{no\ TMS}$]: r = 0.1337, permutation p = 0.2604; softmax temperature [FPl_{TMS} - $FPl_{no\ TMS}$]: r = −0.4486, permutation p = 0.0136; softmax temperature [$Vertex_{TMS}$ - $Vertex_{no\ TMS}$]: r = −0.0625, permutation p = 0.3528; magnitude/probability weighting [FPl_{TMS} - $FPl_{no\ TMS}$]: r = −0.0616, permutation p = 0.3937; magnitude/probability weighting [$Vertex_{TMS}$ - $Vertex_{no\ TMS}$]: r = −0.0141, permutation p = 0.4802; Fig. 6. D-F).

Next, we performed further analysis to demonstrate that the FPl-TMS effect was captured particularly well by the MF_{Mul} - SF_{Add} model. A key feature of this model was that it arbitrates between the multi-feature extraction and simple heuristic processes - where the multi-feature extraction process involves decomposing high-dimensional attribute components and combining them via a multiplicative approach. In contrast, the SF_{Mul} - MF_{Add} model (an alternative model in Fig. 4) involves a "multi-feature" arm that decomposes attributes into multiple features, but integrates them in a simpler additive way. Not only that this model was a poorer fit to participants' behavior overall (Fig. 4. B, 5B), but its computational parameters also failed to capture the FPl-TMS effects. Particularly, a repeated measures two-way ANOVA [Region (FPl vs vertex) and Stimulation (TMS vs no-TMS)] revealed no significant Region × Stimulation interaction on the multiplex coefficients (F (1,18) = 4.0018, p = 0.0608, η^2_P = 0.1819; Fig. S8C, middle panel), softmax temperature (F (1,18) = 0.0777, p = 0.7836, η^2_P = 0.0043; Fig. S9C, middle panel), nor the magnitude/probability weighting (F (1,18) = 0.0009, p = 0.9765, η^2_P = 4.9371 × 10^{-5}; Fig. S10C, middle panel). In addition, the changes in these fitted computational parameters were unrelated to the impaired optimal choice due to FPl-TMS (multiplex coefficient: r = 0.0844, permutation p = 0.3353; magnitude/probability weighting: r = −0.1060, permutation p = 0.3033) although there was a marginally significant correlation between changes in softmax temperature and deviation in percentage of optimal choice (r = −0.3328, permutation p = 0.0504). These results remained similar when each correlation between the choice data and a model parameter was orthogonalized with respect to the other two model parameters (Fig. S8C, bottom panel; Fig. S9C, bottom panel; Fig. S10C, bottom panel).

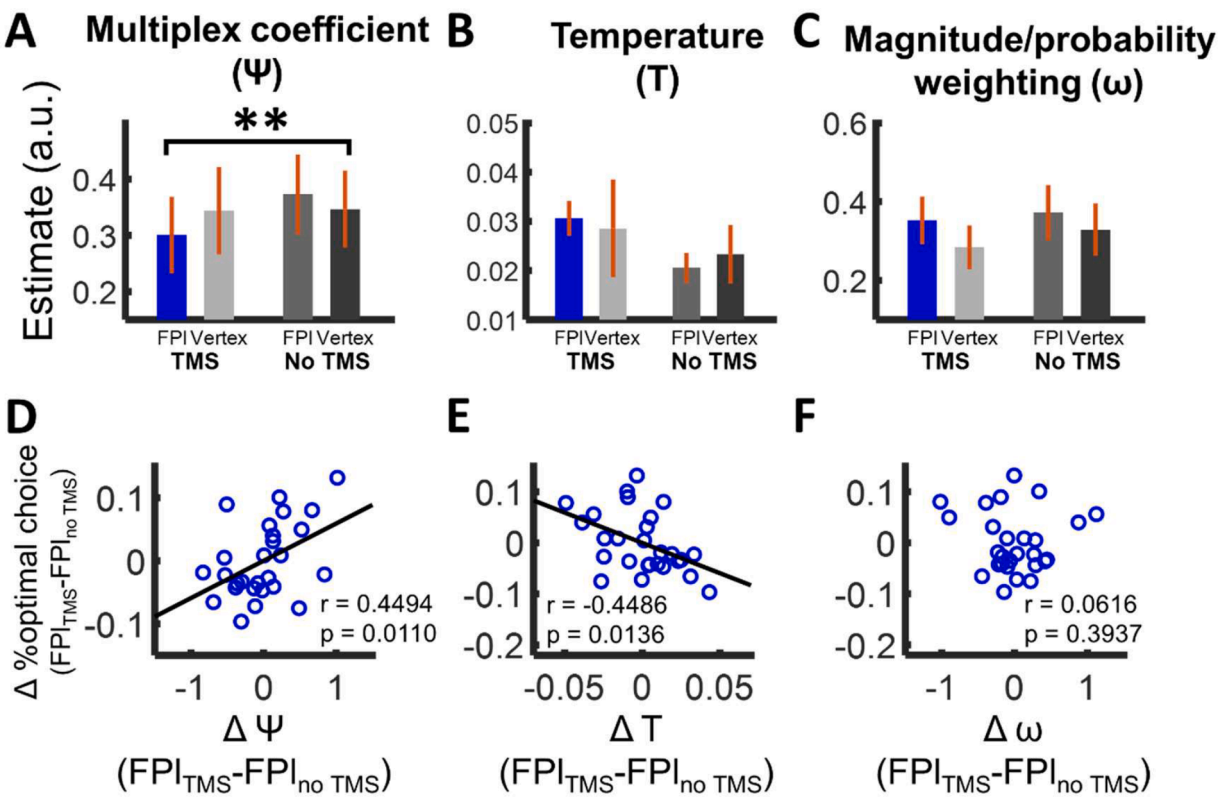

Fig. 6. The FPl-TMS effect on high-dimensional choice was due to the disruption of a multi-feature extraction process. (A) The multiplex coefficient was significantly lower after FPl-TMS than after Vertex-TMS, but no significant difference was found between the two no-TMS conditions in high-dimensional choice. Error bars represent mean ± SEM. $^{**}p < 0.01$ for the Region × Stimulation interaction. In contrast, FPl-TMS had no significant effect on the (B) softmax temperature and (C) magnitude/probability weighting. Individuals that showed greater impairments in percentage optimal choice after FPl-TMS (as opposed to that of the control conditions) also showed (D) greater reductions in multiplex coefficient and (E) greater increases in softmax temperature. (F) The impairment in percentage optimal choice was unrelated to the magnitude/probability weighting.

Similarly, we repeated the same analyses using the $\text{Composite}_{\text{nl}-\text{MF}}$ model, which is half-way between the best-fit MF_{Mul} - SF_{Add} model and the poorer SF_{Mul} - MF_{Add} model - it involves an identical decomposition process of high-dimensional attribute components in both the multiplicative and additive arms. We found that the $\text{Composite}_{\text{nl}-\text{MF}}$ model yielded similar findings to the MF_{Mul} - SF_{Add} model - FPl-TMS gave rise to reduced integration coefficient (Fig. S8B, middle panel), and the impaired optimal choice behavior was related to the reduced integration coefficient (marginally significant; $r = 0.2912$, permutation $p = 0.0798$) and heightened softmax temperature ($r = -0.5097$, permutation $p = 0.0050$) but unrelated to the change in magnitude/probability weighting ($r = 0.0145$, permutation $p = 0.4770$). When each correlation between the choice data and a model parameter was orthogonalized with respect to the other two model parameters to single out each model parameter's contribution, similar results were yielded (Fig. S8B, bottom panel; Fig. S9B, bottom panel; Fig. S10B, bottom panel). These additional results showed that the best-fit MF_{Mul} - SF_{Add} model captures both the overall behavior (Fig. 4. B, 5B) and FPl-TMS effects (Fig. 6) particularly well because it involves all the multi-feature extraction processes in one arm and all the simple heuristic processes in another arm. To summarize, aided by the MF_{Mul} - SF_{Add} model, we showed that the way FPl-TMS impaired high-dimensional choice could be explained mechanistically by a disruption of the multi-feature extraction process such that participants had to rely on simple heuristics.

2.4. *Multi-feature extraction process underlies FPl fMRI signals and high-dimensional choice behavior*

Our findings thus far support the causal role of FPl in decomposing high-dimensional information during decision making by revealing that FPl disruption led to an impairment of a multi-feature extraction process. As such, we should expect that, in the absence of any extrinsic disruption, individuals who exhibit stronger decision signals in FPl should also be more inclined to use more multifaceted strategies. Thus, to complete the functional profile of FPl, in Experiment 3 we further investigated the relationship between decision signals in FPl and the multiplex coefficient. Experiment 3 involved measuring neural activity using fMRI while participants were performing a decision task similar to that of Experiments 1 and 2 (Fig. S11A). Previously, data of Experiment 3 reliably showed a signal in FPl that was specifically related to high-dimensional choice (Law et al., 2023) (Fig. 7. A, left panel). To make it possible to apply the same set of computational models to the behavioral data of Experiment 3, we focused on a subset of the trials in Experiment 3 that was most similar to those in Experiments 1 and 2 (Fig. S11A). We first ensured that a decision signal in FPl can be identified even with this smaller set of trials, as in what was shown using the full set of trials (Law et al., 2023). We performed a timecourse analysis and showed that FPl's activity significantly correlated with the high-dimensional choice value and peaked at approximately 4 s after stimulus onset ($\beta = 0.0772$, $t_{23} = 2.4163$, $p = 0.0240$; Fig. 7. A, right panel, Fig. S11B). This suggests that the selected subset of trials could reliably capture a signal in FPl related to high-dimensional choice.

Next, we applied the same set of computational models to the behavioral data of Experiment 3 and showed, consistently, that the MF_{Mul} - SF_{Add} model best describes participants' high-dimensional choice behavior. Specifically, we followed identical model fitting procedures as in Experiments 1 and 2. Participants' high-dimensional choice behavior was first fitted using the twelve models that are derived from four different attribute functions × three integration functions (as in Fig. 4. A, 5A). A Bayesian model selection showed that

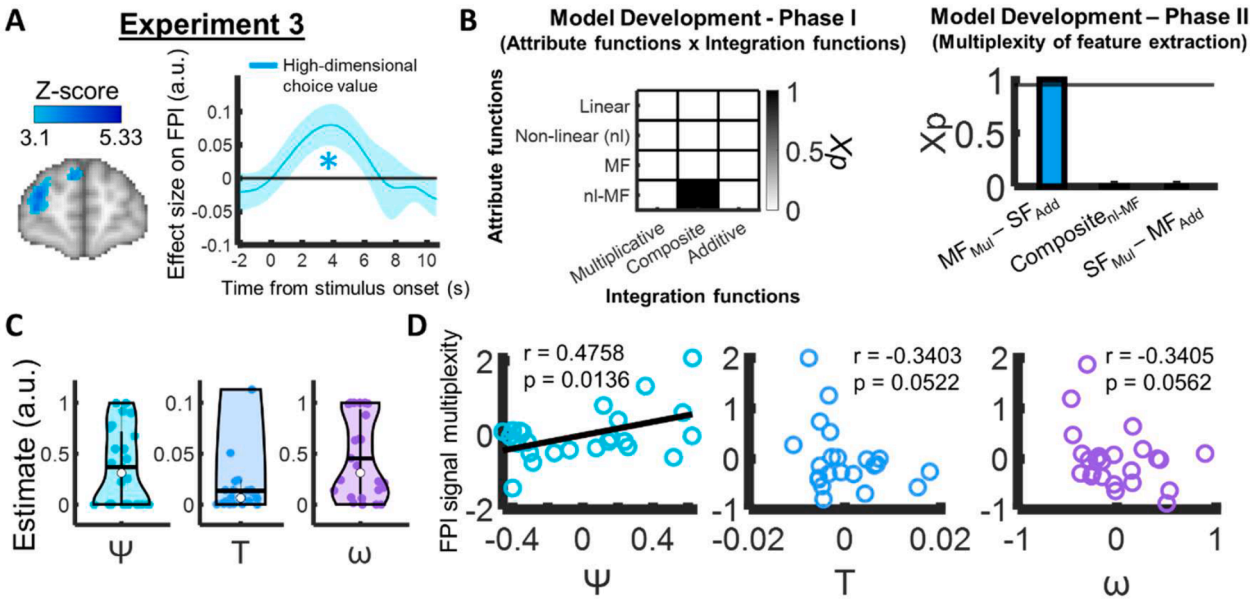

Fig. 7. FPl activity implicated a multi-feature extraction process. (A) Data of Experiment 3 were acquired from a previous fMRI study (Law et al., 2023) which revealed that FPl encodes the high-dimensional choice value during decision making with high-dimensional information (left pane; Adapted from Law et al. 2023). In the current study, we focused on a subset of Experiment 3 trials that was more comparable to the task of Experiments 1 and 2. A time course analysis showed that this smaller set of trials could reliably show a high-dimensional choice value signal in FPl (right panel). Shading represent mean ± SEM. $^*p < 0.05$. (B) The same models applied to the data of Experiments 1 and 2 were applied to the data of Experiment 3. Similar to Figs. 4A and 5A, the $\text{Composite}_{\text{nl}-\text{MF}}$ model outperformed other alternative models in the first phase of model development (left panel). Similar to Figs. 4B and 5B, the MF_{Mul} - SF_{Add} model was the final winning model when two additional models that arbitrates between the multi-feature extraction and simple heuristic processes were considered (right panel). *Xp* = exceedance probability. (C) Violin plots showing the fitted parameters of the MF_{Mul} - SF_{Add} model of individual participants. Vertical black lines represent the interquartile range. Horizontal black lines represent the mean. White circles represent the median. Ψ = multiplex coefficient; ω = magnitude/probability weighting; *T* = softmax temperature. (D) Participants with greater FPl signal multiplexities also showed larger multiplex coefficients (left panel) and lower softmax temperatures (i.e., less stochastic choices; middle panel). While the magnitude/probability weighting were unrelated to the FPl signal multiplexity (right panel).

the $\text{Composite}_{\text{nl}-\text{MF}}$ model outperforms all other models (estimated frequency $Ef = 0.9633$; exceedance probability $Xp = 1.0000$; Fig. 7. B, left panel). Next, we further fitted the MF_{Mul} - SF_{Add} and SF_{Mul} - MF_{Add} models and compared their performance with the $\text{Composite}_{\text{nl}-\text{MF}}$ model. We replicated the results of Experiments 1 and 2 that the MF_{Mul} - SF_{Add} model best describes participants' high-dimensional choice behavior (estimated frequency $Ef = 0.8008$; exceedance probability $Xp = 0.9995$; Fig. 7. B, right panel). The fitted parameters of the MF_{Mul} - SF_{Add} model are shown in Fig. 7C.

We performed the key analysis to scrutinize whether participants' multiplex coefficient was related to their FPl signal during high-dimensional choice. Considering that the decision value of the MF_{Mul} - SF_{Add} model was a combination of a multi-feature extraction process and a simple heuristic (i.e., single-feature extraction), we broke down the FPl signals into these two components (see Experiment 2 - *MF_{Mul} - SF_{Add} model* in Methods). Then, to estimate the contribution of the multi-feature component to the FPl signal (i.e., FPl signal multiplexity), we divided the multi-feature component of the FPl signal by the sum of the multi-feature and single-feature components. Interestingly, we found that the multiplex coefficient was positively correlated with the FPl signal multiplexity ($r = 0.4758$, permutation $p = 0.0136$; Fig. 7. D, left panel). This is in line with the findings of Experiment 1 that greater FPl-TMS induced choice impairment was associated with larger decreases in multiplex coefficient (Fig. S11C). This suggests that the FPl signal reflected the employment of a multi-feature extraction process during decision making. An alternative analysis that separately tested the FPl signals related to the multi-feature and single-feature components also showed that the multiplex coefficient correlated with the multi-feature aspect of the FPl signal more (Fisher transformation $Z = 2.079$, $p = 0.0376$). In addition, we found that the softmax temperature was negatively correlated with the FPl signal multiplexity ($r = -0.5234$, permutation $p = 0.0036$), but the correlation became non-significant when the two rightmost data points (i.e., the two most deviated from the group) were removed from analysis ($r = -0.3403$, permutation $p = 0.0522$; Fig. 7. D, middle panel). We found, surprisingly, a positive correlation between the magnitude/probability weighting and the FPl signal multiplexity ($r = 0.4710$, permutation $p = 0.0060$). This correlation was possibly confounded by the softmax temperature as we identified a marginally significant correlation between them ($r = 0.3530$, permutation $p = 0.0657$). The magnitude/probability weighting was no longer related to the FPl signal multiplexity when the softmax temperature was included as a covariate ($r = -0.3405$, permutation $p = 0.0562$; Fig. 7. D, right panel). Taken the results of our computational modelling, neurostimulation and neuroimaging experiments, we provided evidence from three experiments showing that the FPl is causally involved in a multi-feature extraction process for decomposing choice information.

3. Discussion

This study provides convergent evidence showing FPl's causal role in digesting high-dimensional information during decision making. This was achieved through a combination of TMS, computational modelling, resting-state fMRI, and task-based fMRI. First, using TMS to disrupt the FPl, we found that only high-dimensional choice behavior was impaired but low-dimensional choice behavior was spared (Fig. 2. B). This suggests a specific role of FPl in high-dimensional choice rather than general decision making. Next, to scrutinize the FPl-TMS effect mechanistically, we went through a series of model developments. These modelling work identified two key features for capturing the way people made high-dimensional choice and also for capturing the FPl-TMS effect (Fig. 5. B). First, participants employed a multi-feature extraction process to decompose high-dimensional choice information into low-dimensional parameters in parallel and combine the choice

information multiplicatively. Second, in addition to this multi-feature extraction process, there was a separate simple heuristic for integrating the choice information. A closer inspection showed that disruption of FPl shifted the use of the multi-feature extraction process to simple heuristic (Fig. 6. A). Crucially, the extent of this shift was related to the degree of behavioral impairment in high-dimensional choice after FPl-TMS (Fig. 6. D). Finally, we tested FPl's high-dimensional processing using task-based fMRI. We found that stronger intrinsic FPl signal was associated with more extensive use of the multi-feature extraction process (Fig. 7. D).

Here, we showed that the computations of FPl during high-dimensional choice involves the employment of the multi-feature extraction process. This is in line with previous findings showing that FPl is engaged in parallel processing as depicted in cognitive branching and multitasking (Braver and Bongiolatti, 2002; Donoso et al., 2014; Koechlin et al., 1999) and information integration (Christoff et al., 2003; Kim et al., 2015; Nee and Brown, 2012; Wendelken and Bunge, 2010). Intriguingly, the adjacent dorsolateral prefrontal cortex (dlPFC), a region that is posterior to and functionally connected with FPl (Gilbert et al., 2010; Orr et al., 2015), is often suggested to play a role in high-dimensional processing that is similar to FPl's (e.g., decision making with plenty of information (Reutskaja et al., 2018; Woo et al., 2021) or exploratory decision making (Tomov et al., 2020). However, a closer inspection unveils that although dlPFC and FPl are active in similar tasks, they differ in their capacity of abstraction. DlPFC is pertinent to more concrete processes such as representing the numerosity or overall uncertainty of the choice set. By contrast, FPl is related to more abstract processes such as digesting attribute information (e.g., the subjective value or the relative uncertainty of the options). This is consistent with the view that the lateral prefrontal cortex follows an anterior-posterior gradient, with more anterior regions are involved in processing more abstract information (Badre et al., 2009; Badre and Nee, 2018; Koechlin et al., 2003; Nee and Brown, 2012; Nee and D'Esposito, 2017). Anatomically, dlPFC, which is next to the FPl posteriorly (Petrides and Pandya, 1999), is considered homologous across human and non-human primates (Levy, 2024). In contrast, the FPl is unique in human, which shows distinct sulci and connectivity patterns that are absent in other non-human primates (Amiez et al., 2023; Chau et al., 2025). This might further explain why processes involving higher levels of abstraction such as high-dimensional choice require the evolution of an FPl. On the other hand, despite the functional connectivity between FPl and dlPFC, the findings of the current study as well as previous findings (Law et al., 2023) showed that the engagement of PCC also played an important role in high-dimensional choice. However, the rsFC profiles reveal that the FPl-PCC functional coupling is much stronger than the dlPFC-PCC functional coupling (Neubert et al., 2015). It provides further support of the significance of FPl over dlPFC in high-dimensional choice.

Despite our evidence of the FPl's causal role, the in-depth interplay between the FPl-PCC functional coupling and high-dimensional choice remains unclear in spite of its importance. To better elucidate the functional networks involved in high-dimensional choice, concurrent TMS-fMRI could serve as a potential method in future studies to observe direct causal influences on the connectivity with other brain areas as well as the choice behavior by instantaneous perturbation of FPl. Another limitation of this study, which also applies to TMS research in general, is the selection of an appropriate control to establish the FPl-TMS effect. For example, some studies may opt for subthreshold or sham stimulation, which are poorer at matching the auditory or tactile sensations in the experimental conditions or are limited in inferring spatial specificity of the TMS effect. Other studies may opt for an active control design (such as vertex stimulation, like our study), which runs into problems of potentially modulating other neural networks unintentionally (Jung et al., 2016; Pizem et al., 2022). Thus far there is no evidence of significant influences of vertex stimulation on decision making (e.g., Miyamoto et al., 2021; Zajkowski et al., 2017), suggesting that vertex stimulation as a reasonable choice as a control condition for decision-making studies using TMS.

The ability to make decisions based on high-dimensional information has particularly important adaptive value in the human society. Nonetheless, it remains an unresolved question: what unique features of the human brain enable such high-dimensional processing? The current study has a primary interest in the FPC, which is part of the granular prefrontal cortex is exclusive to primates (Passingham and Wise, 2012). The FPC has a particularly long intrinsic neuronal timescale (Manea et al., 2022), which is a well-suited feature to enable information encoding and integration during complex cognitive processes (Cavanagh et al., 2020). In addition, comparative studies showed that FPC is greatly expanded in the human brain (Semendeferi et al., 2001). This is especially the case in the lateral part of the FPC (i.e., the FPl, the key focus of this study) (Amiez et al., 2023; Neubert et al., 2015, 2014). Here, using TMS to disrupt FPl, we provided causal evidence that the FPl mediates multi-feature extraction for high-dimensional choice information. It is noticeable that the capability of feature extraction by simple averaging alone is observed in many animal species, such as in macaques (Wittmann et al., 2016) and crows (Johnston et al., 2023). Interestingly, we showed that the human FPl involved more than simple averaging - it also estimates the distribution of choice information in terms of variance and skewness. Such capability is particularly useful in many ecological settings when the diversity of reward is as important as the quantity of reward, such as one selecting a job that offers a combination of good salary and social environment instead of the best salary job. This is in line with the view that the FPl enables cognitive branching, the capability of simultaneously engaging in multiple tasks (Koechlin and Hyafil, 2007; Mansouri et al., 2017). Our findings extend this view by showing that the FPl is capable of digesting high-dimensional information into multiple branches of meaningful features for guiding decision making.

Lesions in frontal regions could lead to severe decision-making impairments. However, the clinical implication of FPl lesion was often overlooked in the past due to the poor understanding of its functions. For example, a patient with focal FPC lesion showed normal performance in a wide range of neuropsychological tests known to be sensitive to prefrontal lesions (Hoffman, 2012). Another example concerns a widely discussed case of patient EVR who received frontal excision that covered a large proportion of ventromedial prefrontal cortex (vmPFC) to treat his meningioma. However, often it has been overlooked that EVR's lesion is relatively widespread and extended to the FPl, which is the focus of this study. He was reported to have serious problems in many aspects in everyday life (Eslinger and Damasio, 1985; Shallice and Burgess, 1991). These did not only include simpler routine choices such as being indecisive for where to dine, but also include more critical and complex choices such as poor business investment leading to his bankruptcy and two divorces from his marriages. EVR's problems were often attributed to his vmPFC lesion. This view has been held for years partly because the vmPFC is also widely accepted as the key region for value-based decision making (Bartra et al., 2013; Chau et al., 2018; Clithero and Rangel, 2014; Rushworth et al., 2011). However, how EVR's problems were related to damages beyond the vmPFC, such as the FPl, is rarely discussed. Previously, we reported a double dissociation of FPl and vmPFC in high-dimensional and low-dimensional choices respectively (Law et al., 2023). It is possible that EVR's impairments in making routine choices were more related to his vmPFC lesion whereas his impairments in making more complex choices were more related to his FPl lesion. Moreover, evidence from other lesion studies also suggests FPC patients showed normal performances on various simple cognitive assessments but exhibited impairments in higher-order, complex processes (Dreher et al., 2008; Roca et al., 2011, 2010; Shallice and Burgess, 1991; Urbanski et al., 2016). Here, we further provided causal evidence that FPl disruption only resulted in impairments in high-dimensional choice, but not low-dimensional choice. This study provides a novel perspective to re-evaluate clinical cases of decision-making deficits, such as EVR, by scrutinizing their functioning in high-dimensional processing. Finally,

despite the orthodoxy that modulating FPC activity is difficult in humans (Hogeveen et al., 2022), our findings of FPl-disruption after cTBS provided the foundation for enhancing high-dimensional processing through excitatory TMS over FPl.

4. Materials and methods

4.1. Participants

Seventy-six young healthy adults were recruited in total for all three experiments (Experiment 1: $n = 30$ [60 % males], aged 18–37 years [25.7 ± 4.5]; Experiment 2: $n = 20$ [50 % males], aged 21–39 years [28.2 ± 3.8]; Experiment 3: $n = 26$ [42.3 % males], aged 19–39 years [27.4 ± 5.3]). All participants had no current or history of neurological or psychiatric conditions, and had normal or corrected-to-normal vision. Three participants were excluded in Experient 1 (one withdrew after the TMS preparation session and two were identified left-handed during the TMS preparation session), no participant was excluded in Experiment 2, and two participants were excluded in Experiment 3 (one due to MRI contraindications; another was excluded because his/her fMRI scan was separated into two runs, instead of a single run as in all other participants). As a result, Experiment 1 included twenty-seven participants, Experiment 2 included twenty participants, and Experiment 3 included twenty-four participants. Written informed consent was obtained from each participant before the experiments. Approvals from the ethics committees of The Hong Kong Polytechnic University (Experiments 1 and 2) and University of Oxford (Experiment 3) were obtained for this study.

4.2. Experiment 1

4.2.1. Experimental task

The experimental task was a two-stage decision making task in which the Stage 1 high-dimensional choice determined the options that were offered in the subsequent Stage 2 low-dimensional choice (Fig. 1. B, S1). Specifically, each block began with a Stage 1 high-dimensional choice trial and then followed by up to three Stage 2 low-dimensional choice trials. On each high-dimensional choice trial, participants chose between two collections of gambles with high-dimensional choice information (*Stimulus onset*; response timeframe = 3 s) - each collection was composed of twenty low-dimensional gambles that were associated with different reward magnitudes and probabilities. The reward probabilities of the twenty component gambles were represented by the heights of twenty bars and the average reward magnitude of the component gambles was presented in a number. After selecting a high-dimensional collection, two component gambles from which were pseudo-randomly drawn and offered on the following Stage 2 low-dimensional choice trial. This link between Stage 1 high-dimensional choice and Stage 2 low-dimensional choice was visually illustrated by placing the chosen high-dimensional collection at the screen center (*Delay*; 1.2–1.8 s), and then highlighting the pseudo-randomly drawn component gambles immediately before the onset of each Stage 2 low-dimensional choice trial (*Outcome*; 1.0–1.2 s). Participants subsequently chose between the two low-dimensional gambles offered (*Stimulus onset*; response timeframe = 3 s) - each low-dimensional gamble was characterized by a reward magnitude (presented in a number; ranged from $10 to $100) and a reward probability (represented by the colored area within a bar; ranged from 1/21 to 20/21 chance). A probabilistic reward was then delivered according to the chosen low-dimensional gamble. The decision outcomes of all Stage 2 trials of the same block were disclosed together when all of them were finished (*Outcome*; 0.7–1.2 s). Participants were explicitly instructed that the goal was to maximize their earning, by means of choosing more rewarding options in Stage 1 (high-dimensional choice) and Stage 2 (low-dimensional choice). This task consisted of 100 Stage 1 trials and 100 Stage 2 trials.

4.2.2. Experimental procedure

Experiment 1 involved a preparation session (Session 0) and two TMS sessions (Sessions 1 and 2; Fig. 1. C). In the preparation session, participants received MRI scanning for acquiring their structural images and resting-state fMRI data. Afterwards, they received TMS pulses at a lower intensity than in the experiment proper to familiarize with the TMS (see section *Transcranial magnetic stimulation (TMS)*). They were also instructed on the two-stage decision making task and completed a practice run to familiarize with the task. In the two TMS sessions, TMS was applied either over the key FPl region or the control region vertex. Within each TMS session, participants performed the decision making task twice: once immediately after receiving TMS (i.e., TMS condition) and once without TMS application (i.e., no-TMS condition). The order of the conditions (i.e., TMS over FPl or vertex first; receiving TMS or no TMS first) was counterbalanced across participants. An interval of at least 30 min was inserted between the conditions to prevent carryover of the TMS effect, based on previous findings that the TMS effects diminished rapidly within 30 min even evacuated in ten minutes (Goldsworthy et al., 2012; Miyamoto et al., 2021). Between TMS sessions, there was also an intersession interval of at least seven days apart.

4.2.3. Transcranial magnetic stimulation (TMS)

TMS was applied using a MagVenture MagPro X100 including MagOption (MagVenture, Denmark) with a 75 mm figure-of-eight coil (MagVenture Cool-B65). We used a continuous theta-burst stimulation (cTBS) protocol - 40 s stimulation of 3-pulse bursts at 5 Hz (600 pulses in total) at 80 % of the resting motor threshold (Zajkowski et al., 2017). The resting motor threshold of each participant (mean ± SD: 63.4 % ± 8.5 % of the stimulator output) was assessed in the preparation session - a single pulse stimulation was applied over the left primary motor cortex with the minimal intensity to trigger an involuntary twitch in the right hand in 50 % of the cases (Rossini et al., 2015). Prior to the administration of TMS, for each participant the structural images and head were co-registered via marking with a digitizing pen at six anatomical landmarks (i.e., nasion, inion, left/right preauricular point, left/right exocanthion).

The stimulation coordinate of the key FPl region was determined based on the results of a recent fMRI study on decision making with high-dimensional information (Montreal Neurological Institute [MNI] = [38,52, 22]) (Law et al., 2023). This position is at the edge of the FPl according to the atlas by Neubert and colleagues (2014) that parcellated the frontal cortex using resting-state fMRI and diffusion-weighted imaging data. According to cytoarchitectonic atlas, it lies within Brodmann area 46 and is close to the border between Brodmann areas 46 and 10. According to a recent sulcal atlas, it is at the dorsal paraintermediate frontal sulcus (PIMFS-D) of the FPl, which is present in all human brains studied but absent in 65 % of chimpanzees, all baboons and all macaques (Amiez et al., 2023). The stimulation coordinate of the control region vertex was based on a previous study which employed a similar stimulation protocol (MNI = [0,−34, 72]) (Miyamoto et al., 2021). TMS region localization was guided by the participants' structural images. For each participant, the structural images and the standard MNI template were co-registered using FMRIB's Linear Image Registration Tool (Jenkinson et al., 2002). The intended stimulation coordinates were transformed to individual participant space by which the exact stimulation position for each participant was identified. TMS coil positioning was guided using neuronavigation (TMS Navigator, Localite GmbH, Sankt Augustin, Germany). The TMS coil, with its handle pointing posteriorly, was held tangentially to the skull to minimize the distance between the coil and the cortex.

4.2.4. Computational modelling

The identical computational modelling procedures that were applied to the behavioral data of Experiment 2 were also applied to that of Experiment 1. See Experiment 2 -*Modelling integration process of high-dimensional choice information* for details.

4.2.5. Behavioral analysis

Participants' percentage optimal choice was tested via a three-way repeated-measures ANOVAs [Region (FPl vs vertex), Stimulation (TMS vs no-TMS), and Choice type (high-dimensional vs low-dimensional)] (Fig. 2. B). Two covariates were included to account for individual differences. The first one was the reaction time to account for any influence on choice accuracy due to the trade-off of speed. The other one was the peak resting-state functional connectivity (rsFC) between FPl and PCC (see section *Resting-state functional connectivity analysis*) because the FPl-PCC functional connectivity was found specifically involved in high-dimensional, but not low-dimensional, choice (Law et al., 2023).

Three-way repeated-measures ANOVAs [Region (FPl vs vertex), Stimulation (TMS vs no-TMS), and Choice type (high-dimensional vs low-dimensional)] were performed on the fitted parameters of the MF_{Mul} - SF_{Add} model, namely multiplex coefficient (Ψ), softmax temperature (T), and magnitude/probability weighting (ω) (Fig. 6. A-C). Note that for the low-dimensional choice data, due to the different information structure, the $Composite_{nl}$ model instead of the MF_{Mul} - SF_{Add} model had to be applied and integration coefficient instead of multiplex coefficient was tested. Reaction time and prediction accuracy of the MF_{Mul} - SF_{Add} model were added as covariates. Similar approach was applied to the SF_{Mul} - MF_{Add} model (Fig. S8C, S9C, S10C) and $Composite_{nl-MF}$ model (Fig. S8B, S9B, S10B).

Figs. 6D-F show the correlations between the deviation in percentage optimal choice and the deviation in fitted parameters (i.e., Ψ, T, and ω) of the MF_{Mul} - SF_{Add} model. Each deviation was computed by subtracting the control condition of no-TMS in the FPl session from the FPl-TMS condition. Note that the FPl-PCC rsFC was partialled out since there was a moderate correlation between percentage optimal choice and FPl-PCC rsFC (Fig. 3. B). The same approach was applied to the SF_{Mul} - MF_{Add} model (Fig. S8C, S9C, S10C) and $Composite_{nl-MF}$ model (Fig. S8B, S9B, S10B).

4.2.6. Neuroimaging data acquisition and preprocessing

Neuroimaging data were acquired on a 3 Tesla Siemens Prisma scanner using a 64-channel head coil. Resting-state data were acquired using an echo planar 2D sequence ($3 \times 3 \times 3\ mm^3$ resolution, TR = 3000 ms, TE = 30 ms, flip angle = 85°, phase encoding direction = $A > P$, FOV = $214 \times 214 \times 141\ mm^3$, 47 slices, slice angles = −2.4° [$T > C$] and 0.8° [$T > S$]). Field maps were acquired using a dual echo 2D gradient echo sequence ($3 \times 3 \times 3\ mm^3$ resolution, TR = 520 ms, TE_1 = 4.92 ms, TE_2 = 7.38 ms, flip angle = 60°, phase encoding direction = $R > L$, FOV = $214 \times 214 \times 141\ mm^3$, 47 slices, slice angles = −2.4° [$T > C$] and 0.8° [$T > S$]) to correct for signal distortions. T1-weighted anatomical images were acquired using a 3D MPRAGE sequence ($0.8 \times 0.8 \times 0.8\ mm^3$ resolution, TR = 2500 ms, TE = 2.22 ms, TI = 1120 ms, flip angle = 8°, phase encoding direction = $A > P$, FOV = $240 \times 167 \times 256\ mm^3$, slice angles = 2.5° [$S > C$] and −0.9° [$S > T$]).

Analysis was conducted using FMRIB's Software Library (FSL) (Smith et al., 2004). Preprocessing of the neuroimaging data was performed with the following procedures: brain extraction by Brain Extraction Tool (Smith, 2002), motion correction by using FMRIB's Linear Image Registration Tool (Jenkinson et al., 2002), Gaussian spatial smoothing with fullwidth at half maximum of 5 mm, field map correction for distorted signal (Jenkinson, 2003), and high-pass temporal filtering (3 dB cutoff of 100 s). Neuroimaging data were registered to each participant's high-resolution structural image and then normalized into the standard MNI space (Jenkinson and Smith, 2001).

4.2.7. Resting-state functional connectivity analysis

A resting-state function connectivity (rsFC) analysis was performed for each participant to estimate the strength of functional connectivity between FPl and PCC. It was performed using a univariate general linear model (GLM) approach. The GLM included a single regressor, which is the time course of PCC. The time course of PCC was extracted by creating a spherical mask of 2 mm radius that was centered at the MNI coordinates of (0.7, −47, 26), which was based on the PCC labelled in the Automated anatomical labelling atlas 3 (Rolls et al., 2020). At the contrast level, the regressor of the PCC time course was set as 1. At the group level, FMRIB's local analysis of mixed effects (Beckmann et al., 2003; Woolrich et al., 2004) was applied with outlier deweighting (Woolrich, 2008). A cluster-based thresholding of $Z > 3.1$ and a significance threshold of $p < 0.05$ were used to identify significant clusters (Worsley et al., 1992). The peak of the FPl-PCC rsFC was determined using a FPl mask defined by a previous neuroanatomical study (Neubert et al., 2015).

4.3. Experiment 2

4.3.1. Experimental task

Experiment 2 was conducted for model development to delineate the computational mechanisms underlying high-dimensional choice. Participants performed the identical decision making task as described in the previous section (Experiment 1 - *Experimental task*), except there was no TMS and neuroimaging involved.

4.3.2. Modelling integration process of high-dimensional information

We developed models to describe high-dimensional choice behavior in two phases. In the first phase (Fig. 4, left panel), we considered four attribute functions to model how the choice attributes (i.e., reward magnitude and reward probability) were represented and three integration functions to model how the choice attributes were combined. Combining the attribute functions and integration functions results in twelve models for describing high-dimensional choice behavior. In the second phase (Fig. 4, right panel), we considered that high-dimensional choice could be made based on a combination of a simple heuristic and a multi-feature extraction process. Hence, based on the first phase development, two additional models were developed, namely the MF_{Mul} - SF_{Add} model and SF_{Mul} - MF_{Add} model.

Attribute function 1: linear. Four attribute functions were applied to model how choice attributes were represented. The first attribute function is a linear function in which choice attributes are represented as their objective values:

$$\widehat{Mag}^{i} = Mag^{i} \tag{1}$$

$$\widehat{Prob}^{i} = \frac{1}{20}\sum_{j=1}^{20} Prob_j^i \tag{2}$$

where $\widehat{Mag}^{i}$ and $\widehat{Prob}^{i}$ are the subjective reward magnitude and subjective reward probability respectively. Mag^i is the objective reward magnitude of the i^{th} high-dimensional option (either the option on the left or right). $Prob_j^i$ is the j^{th} individual reward probability in the i^{th} high-dimensional option (each high-dimensional option consisted of a distribution of twenty component reward probabilities).

Attribute function 2: non-linear (nl). Since non-linear transformation is observed in a wide range of cognitive and perceptual processes, another possibility of representation is that the choice attributes are represented in a non-linear manner. To this end, the second attribute function employs the cumulative prospect theory (Tversky and Kahneman, 1992):

$$CPT_{Mag}{}^{i} = \left(Mag^{i}\right)^{\alpha} \tag{3}$$

$$CPT_{Prob_j}{}^{i} = \frac{\left(Prob_j^i\right)^{\gamma}}{\left(\left(Prob_j^i\right)^{\gamma} + \left(1 - Prob_j^i\right)^{\gamma}\right)^{\frac{1}{\gamma}}} \tag{4}$$

$$\widehat{Mag}^{i} = CPT_{Mag}{}^{i} \tag{5}$$

$$\widehat{Prob}^{i} = \frac{1}{20}\sum_{j=1}^{20} CPT_{Prob_j}^{i} \tag{6}$$

where α denotes the sensitivity towards changes in reward magnitude and γ denotes the probability weighting.

Attribute function 3: multi-feature (MF). The third attribute function employs the mean-variance-skewness model (Symmonds et al., 2011; Wright et al., 2013a, 2013b, 2012) by which the representation of the summary statistics (i.e., mean, variance, and skewness) of the high-dimensional options' reward probability distribution is modelled:

$$\widehat{Mag}^{i} = Mag^{i} \tag{7}$$

$$\widehat{Prob}^{i} = \frac{1}{20}\sum_{j=1}^{20} Prob_j^{i} + \rho Var\left(Prob^{i}\right) + \lambda Skew\left(Prob^{i}\right) \tag{8}$$

where ρ and λ are the variance preference and skewness preference respectively.

Attribute function 4: nl-MF. The last attribute function is a combination of MF and nl in which the choice attributes are first transformed by the nl function and subsequently by the MF function:

$$\widehat{Mag}^{i} = CPT_{Mag}{}^{i} \tag{9}$$

$$\widehat{Prob}^{i} = \frac{1}{20}\sum_{j=1}^{20} CPT_{Prob_j}^{i} + \rho Var\left(CPT_{Prob}{}^{i}\right) + \lambda Skew\left(CPT_{Prob}{}^{i}\right) \tag{10}$$

Integration function 1: additive. To model how the choice attributes were combined, three integration functions were. The first one is the additive function. The utility is constituted by the weighted sum of the subjective reward magnitude and subjective reward probability:

$$Utility_{add}{}^{i} = \omega\widehat{Mag}^{i} + (1-\omega)\widehat{Prob}^{i} \tag{11}$$

$$Utility^{i} = Utility_{add}{}^{i} \tag{12}$$

where ω is the magnitude/probability weighting to denote the use of subjective reward magnitude relative to subjective reward probability.

Integration function 2: multiplicative. Alternatively, choice attributes can be combined via the multiplicative function in which the subjective reward magnitude is multiplied by the subjective reward probability to make up the utility of the high-dimensional options:

$$Utility_{mul}{}^{i} = \widehat{Mag}^{i} \times \widehat{Prob}^{i} \tag{13}$$

$$Utility^{i} = Utility_{mul}{}^{i} \tag{14}$$

Integration function 3: composite. Previous studies have shown that it is possible to have a combination of both multiplicative and additive procedures (Bongioanni et al., 2021; Farashahi et al., 2019; Wong et al., 2024). The last integration function is the composite function which involves a push-pull arbitration between multiplicative and additive integration. The utility is derived from a weighted sum of the utility of the multiplicative integration and the utility of the additive integration:

$$Utility^{i} = \Phi Utility_{mul}{}^{i} + (1-\Phi)Utility_{add}{}^{i} \tag{15}$$

where Φ is the integration coefficient to denote the use of multiplicative integration relative to additive integration.

Finally, to model the choice stochasticity of the participants, a softmax function was applied to the utility of each high-dimensional option:

$$P_{choice}{}^{i} = \frac{e^{\frac{Utility^{i}}{T}}}{\sum_{i}^{2} e^{\frac{Utility^{i}}{T}}} \tag{16}$$

where $P_{choice}{}^{i}$ is the choice probability of the i^{th} high-dimensional option. It denotes how likely that high-dimensional option is selected. T is the softmax temperature which denotes the choice stochasticity.

MF_{Mul} - SF_{Add} model. It involves an arbitration between a multi-feature extraction process and a simple heuristic (i.e., single-feature extraction), which is controlled by a multiplex coefficient Ψ:

$$Utility^{i} = \Psi Utility_{Multi-feature}{}^{i} + (1-\Psi)Utility_{Single-feature}{}^{i} \tag{17}$$

where the utility of the i^{th} high-dimensional option (i = left or right) is constituted by the weighted sum of the utility of the multi-feature extraction process and the utility of the simple heuristic. Specifically, the multi-feature extraction process involves decomposing and representing the high-dimensional information of reward probabilities in multiple features, including the mean, variance, and skewness, and then combining with the reward magnitude via a multiplicative integration:

$$Utility_{Multi-feature}{}^{i} = CPT_{Mag}{}^{i} \times Prob_{Multi-feature}{}^{i} \tag{18}$$

$$Prob_{Multi-feature}{}^{i} = \frac{1}{20}\sum_{j=1}^{20} CPT_{Prob_j}^{i} + \rho Var\left(CPT_{Prob}{}^{i}\right) + \lambda Skew\left(CPT_{Prob}{}^{i}\right) \tag{19}$$

where $Prob_{Multi-feature}{}^{i}$ is the reward probability after transformation by the attribute function of MF; CPT_{Prob} is the non-linearly transformed reward probability derived from Eq. (4). In contrast, the simple heuristic only decomposes the reward probability into a single feature (i.e., the mean), and combines with the reward magnitude via an additive integration:

$$Utility_{Single-feature}{}^{i} = \omega CPT_{Mag}{}^{i} + (1-\omega)Prob_{Single-feature}{}^{i} \tag{20}$$

$$Prob_{Single-feature}{}^{i} = \frac{1}{20}\sum_{j=1}^{20} CPT_{Prob_j}^{i} \tag{21}$$

SF_{Mul} - MF_{Add} model. Similar to the MF_{Mul} - SF_{Add} model, the SF_{Mul} - MF_{Add} model also consists of a push-pull system between a multi-feature extraction process and a simple heuristic. However, it has an opposite computational structure: in the multi-feature extraction process attribute information is combined via an additive integration, whereas in the simple heuristic attribute information is combined via a multiplicative integration:

$$Utility^{i} = \Psi Utility_{Multi-feature}{}^{i} + (1-\Psi)Utility_{Single-feature}{}^{i} \tag{22}$$

$$Utility_{Multi-feature}{}^{i} = \omega CPT_{Mag}{}^{i} + (1-\omega)Prob_{Multi-feature}{}^{i} \tag{23}$$

$$Utility_{Single-feature}{}^{i} = CPT_{Mag}{}^{i} \times Prob_{Single-feature}{}^{i} \tag{24}$$

where CPT_{Mag} is the transformed reward magnitude derived from Eq. (3) and $Prob_{Multi-feature}$ is transformed reward probability derived from Eq. (17).

Parameter optimization and model comparison. All models were fitted using MATLAB's fmincon function. For each fitting, 100 sets of random starting points of the model parameters were generated by uniformly sampling from the parameter space. Parameter optimization and good-of-fit of the models were determined by selecting the best-fit results from these sets. After model fitting, the goodness-of-fit between the models were compared using a Bayesian model selection (BMS) procedure (Stephan et al., 2009). Parameters α and γ from the cumulative prospect theory and parameter T from the softmax function were bounded >0 to avoid fitting of negative values. Parameters Ψ, Φ, and ω were bounded between 0 and 1 to model the weighted sum combination.

4.4. Experiment 3

4.4.1. Experimental task

Data of Experiment 3 were acquired from a previous fMRI study (Law et al., 2023), which involved a two-stage decision making task that was highly similar to that in Experiments 1 and 2 (Fig. S11A). The experimental task had the same structure that the Stage 1 high-dimensional choice was followed by the Stage 2 low-dimensional choice. However, Experiment 3 included a few additional features for addressing research questions of the previous study (Law et al., 2023), which are less relevant to the current study. The original design of the task involved four conditions (Gain-Linked, Gain-Unlinked, Loss-Linked and Loss-Unlinked; details explained in Fig. S11A). The Gain-Unlinked condition was most similar to the task used in Experiments 1 and 2. Hence, trials of the Gain-Unlinked condition were selected for analysis in the current Experiment 3.

4.4.2. Computational modelling

The identical computational modelling procedures that were applied to the behavioral data of Experiments 1 and 2 were also applied to that of Experiment 3. See Experiment 2 -*Modelling integration process of high-dimensional choice information* for details.

4.4.3. Neuroimaging data acquisition and preprocessing

Neuroimaging data were acquired using a 3 Tesla Siemens scanner using a 64-channel head coil. Functional MRI data was collected with a multi-band echo planar imaging sequence ($2.5 \times 2.5 \times 2.5$ mm^3 voxel-resolution, TR = 1600 ms, TE_1 = 15 ms, TE_2 = 36.19 ms, TE_3 = 57.38 ms, flip angle = 70°, phase encoding direction = $A > P$, FOV = $210 \times 210 \times 143$ mm^3, 57 slices, slice angle = −30° [$T > C$]). Field maps were acquired using a dual echo 2D gradient echo sequence ($2.5 \times 2.5 \times 2.5$ mm^3 resolution, TR = 590 ms, TE_1 = 4.92 ms, TE_2 = 7.38 ms, flip angle = 46°, phase encoding direction = $A > P$, FOV = $210 \times 210 \times 150$ mm^3, 60 slices, slice angle = −30° [$T > C$]) to correct for signal distortions. T1-weighted structural images were acquired using a 3D MPRAGE sequence ($1 \times 1 \times 1$ mm^3 resolution, TR = 1900 ms, TE = 3.97 ms, TI = 904 ms, flip angle = 8°, phase encoding direction = $R > L$, FOV = $192 \times 174 \times 192$ mm^3, slice angles = transversal).

Analysis was conducted using FMRIB's Software Library (FSL) (Smith et al., 2004). Preprocessing of the neuroimaging data was performed with the following procedures: brain extraction by Brain Extraction Tool (Smith, 2002), motion correction by using FMRIB's Linear Image Registration Tool (Jenkinson et al., 2002), Gaussian spatial smoothing with fullwidth at half maximum of 5 mm, field map correction for distorted signal (Jenkinson, 2003), and high-pass temporal filtering (3 dB cutoff of 100 s). Neuroimaging data were registered to each participant's high-resolution structural image and then normalized into the standard MNI space.

4.4.4. Functional MRI data analysis

Since the data of Experiment 3 were acquired from the subset of Gain-Unlinked trials (Fig. S11A) of a previous study (Law et al., 2023), we first performed the same analysis as in the previous study but testing on this subset only to test whether FPl signals were reliably related to the high-dimensional choice (Fig. 7A, right panel). It was achieved by a region-of-interest (ROI) analysis to regress the FPl activity against the high-dimensional choice value, (i.e., the difference in the decision value between the chosen and unchosen high-dimensional options derived from a neural network previously reported (Law et al., 2023)). Specifically, FPl activity was first extracted by creating a spherical mask of 3 mm radius. To avoid circularity, the mask was derived from a different study that suggests FPl is involved in value-based decision making (Zajkowski et al., 2017). A ten-time upsampling was applied to the extracted FPl activity by cubic spline interpolation and time-locked to stimulus onset in Stage 1 high-dimensional choice. A GLM was performed to regress the FPl activity against the high-dimensional choice value. Specifically, the GLM was performed at each time point for each participant, by which time courses of beta weight for the high-dimensional choice value were obtained. Group time courses were then acquired by averaging the beta weight time courses from all participants and the significance of each peak in the group time courses was tested. It was performed by extracting the size of each peak from every participant and then running a one-sample *t*-test against zero. To avoid any bias in determining the size of the peaks, a leave-one-participant-out procedure was applied (Chau et al., 2015; Trudel et al., 2021). First, the time window for extraction of each peak was defined by its full-width half-maximum in the group time course. Within this time window, the peak's position after excluding the betas weights of a given participant from the group time course defined the time point of peak extraction for that participant. This leave-one-participant-out procedure was repeated for all participants to extract the peaks for statistical tests.

To test whether the push-pull mechanism of arbitrating between the multi-feature extraction and the simple heuristic as described in the MF_{Mul} - SF_{Add} model (Fig. 4. B, 5B) was related to FPl activity, we performed another ROI analysis. Specifically, FPl activity was regressed against the $Utility_{Multi\text{-}feature}$ and $Utility_{Single\text{-}feature}$ derived from the MF_{Mul} - SF_{Add} model respectively. FPl signal multiplexity was then computed by dividing the peak $Utility_{Multi\text{-}feature}$ effect by the sum of peak $Utility_{Multi\text{-}feature}$ and $Utility_{Single\text{-}feature}$ effects. Finally, correlation between the FPl signal multiplexity and the fitted parameters from the MF_{Mul} - SF_{Add} model of each participant was tested, controlled for the prediction accuracy of the MF_{Mul} - SF_{Add} model to avoid any confounding effect due to individuals'goodness-of-fit.

Data and code availability

All original code and reported data can be found at doi: 10.17632/rdm7yx5bmm.1.

Any additional information required to reanalyze the data reported in this paper is available from the lead contact upon request.

CRediT authorship contribution statement

Chun-Kit Law: Writing – review & editing, Writing – original draft, Visualization, Methodology, Investigation, Data curation, Conceptualization. **Nicole H.L. Wong:** Writing – review & editing. **Jing Jun Wong:** Writing – review & editing. **Evelyn Y.H. Huang:** Investigation. **Rongjun Yu:** Writing – review & editing, Funding acquisition, Conceptualization. **Bolton K.H. Chau:** Writing – review & editing, Visualization, Supervision, Funding acquisition, Conceptualization.

Declaration of competing interest

The authors declare that they have no known competing financial interests or personal relationships that could have appeared to influence the work reported in this paper.

Acknowledgments

We thank Nils Kolling for his help in logistics of data collection during Experiment 3 and Tommy L.H. Lam for providing TMS technical support. This work was supported by the Hong Kong Research Grants Council (C5001-23Y; PDFS2425-5H03) and PolyU Project of Strategic Importance.

Supplementary materials

Supplementary material associated with this article can be found, in the online version, at doi:10.1016/j.neuroimage.2026.121758.

References

Aichelburg, C., Urbanski, M., Thiebaut De Schotten, M., Humbert, F., Levy, R., Volle, E., 2016. Morphometry of left frontal and temporal poles predicts analogical reasoning abilities. Cereb. Cortex. 26, 915–932. https://doi.org/10.1093/cercor/bhu254.

Amiez, C., Sallet, J., Giacometti, C., Verstraete, C., Gandaux, C., Morel-Latour, V., Meguerditchian, A., Hadj-Bouziane, F., Ben Hamed, S., Hopkins, W.D., Procyk, E., Wilson, C.R.E., Petrides, M., 2023. A revised perspective on the evolution of the lateral frontal cortex in primates. Sci. Adv. 9, eadf9445. https://doi.org/10.1126/sciadv.adf9445.

Badre, D., Hoffman, J., Cooney, J.W., D'Esposito, M., 2009. Hierarchical cognitive control deficits following damage to the human frontal lobe. Nat. Neurosci. 12, 515–522. https://doi.org/10.1038/nn.2277.

Badre, D., Nee, D.E., 2018. Frontal cortex and the hierarchical control of behavior. Trends Cogn. Sci. (Regul. Ed.) 22, 170–188. https://doi.org/10.1016/j.tics.2017.11.005.

Bartra, O., McGuire, J.T., Kable, J.W., 2013. The valuation system: a coordinate-based meta-analysis of BOLD fMRI experiments examining neural correlates of subjective value. Neuroimage 76, 412–427. https://doi.org/10.1016/j.neuroimage.2013.02.063.

Beckmann, C.F., Jenkinson, M., Smith, S.M., 2003. General multilevel linear modeling for group analysis in FMRI. Neuroimage 20, 1052–1063. https://doi.org/10.1016/S1053-8119(03)00435-X.

Blanchard, T.C., Hayden, B.Y., 2014. Neurons in dorsal anterior cingulate cortex signal postdecisional variables in a foraging task. J. Neurosci. 34, 646–655. https://doi.org/10.1523/JNEUROSCI.3151-13.2014.

Bongioanni, A., Folloni, D., Verhagen, L., Sallet, J., Klein-Flügge, M.C., Rushworth, M.F.S., 2021. Activation and disruption of a neural mechanism for novel choice in monkeys. Nature 591, 270–274. https://doi.org/10.1038/s41586-020-03115-5.

Boorman, E.D., Behrens, T.E., Rushworth, M.F., 2011. Counterfactual choice and learning in a neural network centered on Human lateral frontopolar cortex. PLoS. Biol. 9, e1001093. https://doi.org/10.1371/journal.pbio.1001093.

Boorman, E.D., Behrens, T.E.J., Woolrich, M.W., Rushworth, M.F.S., 2009. How green is the grass on the other side? Frontopolar cortex and the evidence in favor of alternative courses of action. Neuron 62, 733–743. https://doi.org/10.1016/j.neuron.2009.05.014.

Braver, T.S., Bongiolatti, S.R., 2002. The role of frontopolar cortex in subgoal processing during working memory. Neuroimage 15, 523–536. https://doi.org/10.1006/nimg.2001.1019.

Cavanagh, S.E., Hunt, L.T., Kennerley, S.W., 2020. A diversity of intrinsic timescales underlie neural computations. Front. Neural Circuits. 14, 615626. https://doi.org/10.3389/fncir.2020.615626.

Chau, B.K.H., Jarvis, H., Law, C.-K., Chong, T.T.-J., 2018. Dopamine and reward: a view from the prefrontal cortex. Behav. Pharmacol. 29, 569–583. https://doi.org/10.1097/FBP.0000000000000424.

Chau, B.K.H., Law, C.-K., To, J.Y.L., Shum, D.H.K., Mars, R.B., 2025. Complex functions of human lateral frontopolar cortex. Brain 148, 3833–3843. https://doi.org/10.1093/brain/awaf289.

Chau, B.K.H., Sallet, J., Papageorgiou, G.K., Noonan, M.P., Bell, A.H., Walton, M.E., Rushworth, M.F.S., 2015. Contrasting roles for orbitofrontal cortex and amygdala in credit assignment and learning in macaques. Neuron 87, 1106–1118. https://doi.org/10.1016/j.neuron.2015.08.018.

Christoff, K., Ream, J.M., Geddes, L.P.T., Gabrieli, J.D.E., 2003. Evaluating self-generated information: anterior prefrontal contributions to Human cognition. Behav. Neurosci. 117, 1161–1168. https://doi.org/10.1037/0735-7044.117.6.1161.

Clithero, J.A., Rangel, A., 2014. Informatic parcellation of the network involved in the computation of subjective value. Soc. Cogn. Affect. Neurosci. 9, 1289–1302. https://doi.org/10.1093/scan/nst106.

Daw, N.D., O'Doherty, J.P., Dayan, P., Seymour, B., Dolan, R.J., 2006. Cortical substrates for exploratory decisions in humans. Nature 441, 876–879. https://doi.org/10.1038/nature04766.

Doll, B.B., Duncan, K.D., Simon, D.A., Shohamy, D., Daw, N.D., 2015. Model-based choices involve prospective neural activity. Nat. Neurosci. 18, 767–772. https://doi.org/10.1038/nn.3981.

Donoso, M., Collins, A.G.E., Koechlin, E., 2014. Foundations of human reasoning in the prefrontal cortex. Science (1979) 344, 1481–1486. https://doi.org/10.1126/science.1252254.

Dreher, J.-C., Koechlin, E., Tierney, M., Grafman, J., 2008. Damage to the Fronto-polar cortex is associated with impaired multitasking. PLoS. One 3, e3227. https://doi.org/10.1371/journal.pone.0003227.

Eslinger, P.J., Damasio, A.R., 1985. Severe disturbance of higher cognition after bilateral frontal lobe ablation: patient EVR. Neurology. 35, 1731–1741. https://doi.org/10.1212/wnl.35.12.1731.

Farashahi, S., Donahue, C.H., Hayden, B.Y., Lee, D., Soltani, A., 2019. Flexible combination of reward information across primates. Nat. Hum. Behav. 3, 1215–1224. https://doi.org/10.1038/s41562-019-0714-3.

Fouragnan, E.F., Chau, B.K.H., Folloni, D., Kolling, N., Verhagen, L., Klein-Flügge, M., Tankelevitch, L., Papageorgiou, G.K., Aubry, J.-F., Sallet, J., Rushworth, M.F.S., 2019. The macaque anterior cingulate cortex translates counterfactual choice value into actual behavioral change. Nat. Neurosci. 22, 797–808. https://doi.org/10.1038/s41593-019-0375-6.

Fox, M.D., Buckner, R.L., White, M.P., Greicius, M.D., Pascual-Leone, A., 2012. Efficacy of transcranial magnetic stimulation targets for depression is related to intrinsic functional connectivity with the subgenual cingulate. Biol. Psychiatry 72, 595–603. https://doi.org/10.1016/j.biopsych.2012.04.028.

Gilbert, S.J., Gonen-Yaacovi, G., Benoit, R.G., Volle, E., Burgess, P.W., 2010. Distinct functional connectivity associated with lateral versus medial rostral prefrontal cortex: a meta-analysis. Neuroimage 53, 1359–1367. https://doi.org/10.1016/j.neuroimage.2010.07.032.

Goldsworthy, M.R., Pitcher, J.B., Ridding, M.C., 2012. A comparison of two different continuous theta burst stimulation paradigms applied to the human primary motor cortex. Clin. Neurophysiol. 123, 2256–2263. https://doi.org/10.1016/j.clinph.2012.05.001.

Hawco, C., Voineskos, A.N., Steeves, J.K.E., Dickie, E.W., Viviano, J.D., Downar, J., Blumberger, D.M., Daskalakis, Z.J., 2018. Spread of activity following TMS is related to intrinsic resting connectivity to the salience network: a concurrent TMS-fMRI study. Cortex 108, 160–172. https://doi.org/10.1016/j.cortex.2018.07.010.

Hayden, B.Y., Pearson, J.M., Platt, M.L., 2011. Neuronal basis of sequential foraging decisions in a patchy environment. Nat. Neurosci. 14, 933–939. https://doi.org/10.1038/nn.2856.

Hoffman, M., 2012. Isolated frontopolar cortex lesion: a case study. Cogn. Behav. Neurol. 25.

Hogeveen, J., Medalla, M., Ainsworth, M., Galeazzi, J.M., Hanlon, C.A., Mansouri, F.A., Costa, V.D., 2022. What does the frontopolar cortex contribute to goal-directed cognition and action? J. Neurosci. 42, 8508–8513. https://doi.org/10.1523/JNEUROSCI.1143-22.2022.

Hunt, L.T., Kolling, N., Soltani, A., Woolrich, M.W., Rushworth, M.F.S., Behrens, T.E.J., 2012. Mechanisms underlying cortical activity during value-guided choice. Nat. Neurosci. 15, 470–476. https://doi.org/10.1038/nn.3017.

Jenkinson, M., 2003. Fast, automated,N-dimensional phase-unwrapping algorithm. Magn. Reson. Med. 49, 193–197. https://doi.org/10.1002/mrm.10354.

Jenkinson, M., Bannister, P., Brady, M., Smith, S., 2002. Improved optimization for the robust and accurate linear registration and motion correction of brain images. Neuroimage 17, 825–841. https://doi.org/10.1006/nimg.2002.1132.

Jenkinson, M., Smith, S., 2001. A global optimisation method for robust affine registration of brain images. Med. Image Anal. 5, 143–156. https://doi.org/10.1016/S1361-8415(01)00036-6.

Jocham, G., Furlong, P.M., Kröger, I.L., Kahn, M.C., Hunt, L.T., Behrens, T.E.J., 2014. Dissociable contributions of ventromedial prefrontal and posterior parietal cortex to value-guided choice. Neuroimage 100, 498–506. https://doi.org/10.1016/j.neuroimage.2014.06.005.

Johnston, M., Brecht, K.F., Nieder, A., 2023. Crows flexibly apply statistical inferences based on previous experience. Curr. Biol. 33, 3238–3243. https://doi.org/10.1016/j.cub.2023.06.023 e3.

Jung, J., Bungert, A., Bowtell, R., Jackson, S.R., 2016. Vertex stimulation as a control site for transcranial Magnetic stimulation: a concurrent TMS/fMRI study. Brain Stimul. 9, 58–64. https://doi.org/10.1016/j.brs.2015.09.008.

Kim, C., Kroger, J.K., Calhoun, V.D., Clark, V.P., 2015. The role of the frontopolar cortex in manipulation of integrated information in working memory. Neurosci. Lett. 595, 25–29. https://doi.org/10.1016/j.neulet.2015.03.044.

Koechlin, E., 2014. An evolutionary computational theory of prefrontal executive function in decision-making. Phil. Trans. R. Soc. B 369, 20130474. https://doi.org/10.1098/rstb.2013.0474.

Koechlin, E., 2011. Frontal pole function: what is specifically human? Trends Cogn. Sci. (Regul. Ed.) 15, 241. https://doi.org/10.1016/j.tics.2011.04.005.

Koechlin, E., Basso, G., Pietrini, P., Panzer, S., Grafman, J., 1999. The role of the anterior prefrontal cortex in human cognition. Nature 399, 148–151. https://doi.org/10.1038/20178.

Koechlin, E., Hyafil, A., 2007. Anterior prefrontal function and the limits of Human decision-making. Science (1979) 318, 594–598. https://doi.org/10.1126/science.1142995.

Koechlin, E., Ody, C., Kouneiher, F., 2003. The architecture of cognitive control in the Human prefrontal cortex. Science (1979) 302, 1181–1185. https://doi.org/10.1126/science.1088545.

Kolling, N., Behrens, T.E.J., Mars, R.B., Rushworth, M.F.S., 2012. Neural mechanisms of foraging. Science (1979) 336, 95–98. https://doi.org/10.1126/science.1216930.

Kolling, N., Wittmann, M., Rushworth, M.F.S., 2014. Multiple neural mechanisms of decision making and their competition under changing risk pressure. Neuron 81, 1190–1202. https://doi.org/10.1016/j.neuron.2014.01.033.

Law, C.-K., Kolling, N., Chan, C.C.H., Chau, B.K.H., 2023. Frontopolar cortex represents complex features and decision value during choice between environments. Cell Rep. 42, 112555. https://doi.org/10.1016/j.celrep.2023.112555.

Levy, R., 2024. The prefrontal cortex: from monkey to man. Brain 147, 794–815. https://doi.org/10.1093/brain/awad389.

Manea, A.M., Zilverstand, A., Ugurbil, K., Heilbronner, S.R., Zimmermann, J., 2022. Intrinsic timescales as an organizational principle of neural processing across the whole rhesus macaque brain. Elife 11, e75540. https://doi.org/10.7554/eLife.75540.

Mansouri, F.A., Koechlin, E., Rosa, M.G.P., Buckley, M.J., 2017. Managing competing goals - a key role for the frontopolar cortex. Nat. Rev. Neurosci. 18, 645–657. https://doi.org/10.1038/nrn.2017.111.

Miyamoto, K., Trudel, N., Kamermans, K., Lim, M.C., Lazari, A., Verhagen, L., Wittmann, M.K., Rushworth, M.F.S., 2021. Identification and disruption of a neural mechanism for accumulating prospective metacognitive information prior to decision-making. Neuron 109, 1396–1408. https://doi.org/10.1016/j.neuron.2021.02.024. .e7.

Nee, D.E., Brown, J.W., 2012. Rostral-caudal gradients of abstraction revealed by multi-variate pattern analysis of working memory. Neuroimage 63, 1285–1294. https://doi.org/10.1016/j.neuroimage.2012.08.034.

Nee, D.E., D'Esposito, M., 2017. Causal evidence for lateral prefrontal cortex dynamics supporting cognitive control. Elife 6, e28040. https://doi.org/10.7554/eLife.28040.

Nee, D.E., D'Esposito, M., 2016. The hierarchical organization of the lateral prefrontal cortex. Elife 5, e12112. https://doi.org/10.7554/eLife.12112.
Neubert, F.-X., Mars, R.B., Sallet, J., Rushworth, M.F.S., 2015. Connectivity reveals relationship of brain areas for reward-guided learning and decision making in human and monkey frontal cortex. Proc. Natl. Acad. Sci. USA 112, E2695–E2704. https://doi.org/10.1073/pnas.1410767112.
Neubert, F.-X., Mars, R.B., Thomas, A.G., Sallet, J., Rushworth, M.F.S., 2014. Comparison of Human ventral frontal cortex areas for cognitive control and language with areas in monkey frontal cortex. Neuron 81, 700–713. https://doi.org/10.1016/j.neuron.2013.11.012.
Orr, J.M., Smolker, H.R., Banich, M.T., 2015. Organization of the Human frontal pole revealed by large-scale DTI-based connectivity: implications for control of behavior. PLoS. One 10, e0124797. https://doi.org/10.1371/journal.pone.0124797.
Passingham, R.E., Wise, S.P., 2012. Evolution of the primate prefrontal cortex. The Neurobiology of the Prefrontal Cortex: Anatomy, Evolution, and the Origin of Insight. Oxford University Press. https://doi.org/10.1093/acprof:osobl/9780199552917.001.0001.
Petrides, M., Pandya, D.N., 1999. Dorsolateral prefrontal cortex: comparative cytoarchitectonic analysis in the human and the macaque brain and corticocortical connection patterns. Eur. J. Neurosci. 11, 1011–1036. https://doi.org/10.1046/j.1460-9568.1999.00518.x.
Pizem, D., Novakova, L., Gajdos, M., Rektorova, I., 2022. Is the vertex a good control stimulation site? Theta burst stimulation in healthy controls. J. Neural Transm. 129, 319–329. https://doi.org/10.1007/s00702-022-02466-9.
Raja Beharelle, A., Polania, R., Hare, T.A., Ruff, C.C., 2015. Transcranial stimulation over frontopolar cortex elucidates the choice attributes and neural mechanisms used to resolve exploration-exploitation trade-offs. J. Neurosci. 35, 14544–14556. https://doi.org/10.1523/JNEUROSCI.2322-15.2015.
Reutskaja, E., Lindner, A., Nagel, R., Andersen, R.A., Camerer, C.F., 2018. Choice overload reduces neural signatures of choice set value in dorsal striatum and anterior cingulate cortex. Nat. Hum. Behav. 2, 925–935. https://doi.org/10.1038/s41562-018-0440-2.
Roca, M., Parr, A., Thompson, R., Woolgar, A., Torralva, T., Antoun, N., Manes, F., Duncan, J., 2010. Executive function and fluid intelligence after frontal lobe lesions. Brain 133, 234–247. https://doi.org/10.1093/brain/awp269.
Roca, M., Torralva, T., Gleichgerrcht, E., Woolgar, A., Thompson, R., Duncan, J., Manes, F., 2011. The role of area 10 (BA10) in human multitasking and in social cognition: a lesion study. Neuropsychologia 49, 3525–3531. https://doi.org/10.1016/j.neuropsychologia.2011.09.003.
Rolls, E.T., Huang, C.-C., Lin, C.-P., Feng, J., Joliot, M., 2020. Automated anatomical labelling atlas 3. Neuroimage 206, 116189. https://doi.org/10.1016/j.neuroimage.2019.116189.
Rossini, P.M., Burke, D., Chen, R., Cohen, L.G., Daskalakis, Z., Di Iorio, R., Di Lazzaro, V., Ferreri, F., Fitzgerald, P.B., George, M.S., Hallett, M., Lefaucheur, J.P., Langguth, B., Matsumoto, H., Miniussi, C., Nitsche, M.A., Pascual-Leone, A., Paulus, W., Rossi, S., Rothwell, J.C., Siebner, H.R., Ugawa, Y., Walsh, V., Ziemann, U., 2015. Non-invasive electrical and magnetic stimulation of the brain, spinal cord, roots and peripheral nerves: basic principles and procedures for routine clinical and research application. An updated report from an I.F.C.N. Committee. Clin. Neurophysiol. 126, 1071–1107. https://doi.org/10.1016/j.clinph.2015.02.001.
Rushworth, M.F.S., Noonan, M.P., Boorman, E.D., Walton, M.E., Behrens, T.E., 2011. Frontal cortex and reward-guided learning and decision-making. Neuron 70, 1054–1069. https://doi.org/10.1016/j.neuron.2011.05.014.
Semendeferi, K., Armstrong, E., Schleicher, A., Zilles, K., Van Hoesen, G.W., 2001. Prefrontal cortex in humans and apes: a comparative study of area 10. Am. J. Phys. Anthropol. 114, 224–241. https://doi.org/10.1002/1096-8644(200103)114:3%253C224::AID-AJPA1022%253E3.0.CO;2-I.
Shallice, T., Burgess, P.W., 1991. Deficits in strategy application following frontal lobe damage in man. Brain 114, 727–741. https://doi.org/10.1093/brain/114.2.727.
Smith, S.M., 2002. Fast robust automated brain extraction. Hum. Brain Mapp. 17, 143–155. https://doi.org/10.1002/hbm.10062.
Smith, S.M., Jenkinson, M., Woolrich, M.W., Beckmann, C.F., Behrens, T.E.J., Johansen-Berg, H., Bannister, P.R., De Luca, M., Drobnjak, I., Flitney, D.E., Niazy, R.K., Saunders, J., Vickers, J., Zhang, Y., De Stefano, N., Brady, J.M., Matthews, P.M., 2004. Advances in functional and structural MR image analysis and implementation as FSL. Neuroimage 23, S208–S219. https://doi.org/10.1016/j.neuroimage.2004.07.051.
Soleimani, G., Joutsa, J., Moussawi, K., Siddiqi, S.H., Kuplicki, R., Bikson, M., Paulus, M. P., Fox, M.D., Hanlon, C.A., Ekhtiari, H., 2024. Converging evidence for frontopolar cortex as a target for neuromodulation in addiction treatment. Am. J. Psychiatry 181, 100–114. https://doi.org/10.1176/appi.ajp.20221022.
Stephan, K.E., Penny, W.D., Daunizeau, J., Moran, R.J., Friston, K.J., 2009. Bayesian model selection for group studies. Neuroimage 46, 1004–1017. https://doi.org/10.1016/j.neuroimage.2009.03.025.
Strait, C.E., Blanchard, T.C., Hayden, B.Y., 2014. Reward value comparison via mutual inhibition in ventromedial prefrontal cortex. Neuron 82, 1357–1366. https://doi.org/10.1016/j.neuron.2014.04.032.
Symmonds, M., Wright, N.D., Bach, D.R., Dolan, R.J., 2011. Deconstructing risk: separable encoding of variance and skewness in the brain. Neuroimage 58, 1139–1149. https://doi.org/10.1016/j.neuroimage.2011.06.087.
Tomov, M.S., Truong, V.Q., Hundia, R.A., Gershman, S.J., 2020. Dissociable neural correlates of uncertainty underlie different exploration strategies. Nat. Commun. 11, 2371. https://doi.org/10.1038/s41467-020-15766-z.
Trudel, N., Scholl, J., Klein-Flügge, M.C., Fouragnan, E., Tankelevitch, L., Wittmann, M. K., Rushworth, M.F.S., 2021. Polarity of uncertainty representation during exploration and exploitation in ventromedial prefrontal cortex. Nat. Hum. Behav. 5, 83–98. https://doi.org/10.1038/s41562-020-0929-3.
Tversky, A., Kahneman, D., 1992. Advances in prospect theory: cumulative representation of uncertainty. J. Risk. Uncertain. 5, 297–323. https://doi.org/10.1007/BF00122574.
Urbanski, M., Bréchemier, M.-L., Garcin, B., Bendetowicz, D., Thiebaut De Schotten, M., Foulon, C., Rosso, C., Clarençon, F., Dupont, S., Pradat-Diehl, P., Labeyrie, M.-A., Levy, R., Volle, E., 2016. Reasoning by analogy requires the left frontal pole: lesion-deficit mapping and clinical implications. Brain 139, 1783–1799. https://doi.org/10.1093/brain/aww072.
Volle, E., Gilbert, S.J., Benoit, R.G., Burgess, P.W., 2010. Specialization of the rostral prefrontal cortex for distinct analogy processes. Cerebral Cortex 20, 2647–2659. https://doi.org/10.1093/cercor/bhq012.
Wendelken, C., Bunge, S.A., 2010. Transitive inference: distinct contributions of rostrolateral prefrontal cortex and the hippocampus. J. Cogn. Neurosci. 22, 837–847. https://doi.org/10.1162/jocn.2009.21226.
Wittmann, M.K., Kolling, N., Akaishi, R., Chau, B.K.H., Brown, J.W., Nelissen, N., Rushworth, M.F.S., 2016. Predictive decision making driven by multiple time-linked reward representations in the anterior cingulate cortex. Nat. Commun. 7, 12327. https://doi.org/10.1038/ncomms12327.
Wong, J.J., Bongioanni, A., Rushworth, M.F., Chau, B.K., 2024. Distractor effects in decision making are related to the individual's style of integrating choice attributes. https://doi.org/10.7554/eLife.91102.2.
Woo, T.-F., Law, C.-K., Ting, K.-H., Chan, C.C.H., Kolling, N., Watanabe, K., Chau, B.K.H., 2021. Distinct causal influences of dorsolateral prefrontal cortex and posterior parietal cortex in multiple-option decision making. Cerebral Cortex bhab 278. https://doi.org/10.1093/cercor/bhab278.
Woolrich, M.W., 2008. Robust group analysis using outlier inference. Neuroimage 41, 286–301. https://doi.org/10.1016/j.neuroimage.2008.02.042.
Woolrich, M.W., Behrens, T.E.J., Beckmann, C.F., Jenkinson, M., Smith, S.M., 2004. Multilevel linear modelling for FMRI group analysis using bayesian inference. Neuroimage 21, 1732–1747. https://doi.org/10.1016/j.neuroimage.2003.12.023.
Worsley, K.J., Evans, A.C., Marrett, S., Neelin, P., 1992. A three-dimensional statistical analysis for CBF activation studies in Human brain. J. Cereb. Blood Flow Metab. 12, 900–918. https://doi.org/10.1038/jcbfm.1992.127.
Wright, N.D., Symmonds, M., Dolan, R.J., 2013a. Distinct encoding of risk and value in economic choice between multiple risky options. Neuroimage 81, 431–440. https://doi.org/10.1016/j.neuroimage.2013.05.023.
Wright, N.D., Symmonds, M., Hodgson, K., Fitzgerald, T.H.B., Crawford, B., Dolan, R.J., 2012. Approach-avoidance processes contribute to dissociable impacts of risk and loss on choice. J. Neurosci. 32, 7009–7020. https://doi.org/10.1523/JNEUROSCI.0049-12.2012.
Wright, N.D., Symmonds, M., Morris, L.S., Dolan, R.J., 2013b. Dissociable influences of skewness and valence on economic choice and neural activity. PLoS. One 8, e83454. https://doi.org/10.1371/journal.pone.0083454.
Zajkowski, W.K., Kossut, M., Wilson, R.C., 2017. A causal role for right frontopolar cortex in directed, but not random, exploration. Elife 6, e27430. https://doi.org/10.7554/eLife.27430.